Connectional Hierarchy in Human Brain Revealed by Individual Variability of Functional Network Edges

Hang Yang[1,#], Guowei Wu[1,2,#], Yaoxin Li[1,3], Yiyao Ma[1], Runsen Chen[4], Adam Pines[5], Ting Xu[6], Valerie J. Sydnor[7,8], Theodore D. Satterthwaite[7,8], Zaixu Cui[1,*]

[1]Chinese Institute for Brain Research, Beijing, 102206, China
[2]CAS Key Laboratory of Behavioral Science, Institute of Psychology, Chinese Academy of Sciences, Beijing, 100101, China
[3]Michigan Neuroscience Institute, University of Michigan, Ann Arbor, MI 48109, USA
[4]Vanke School of Public Health, Tsinghua University, Beijing, China
[5]Psychiatry and Behavioral Sciences, Stanford School of Medicine, Stanford University, Stanford, California, USA
[6]Center for the Developing Brain, Child Mind Institute, New York, NY 10022, USA
[7]Penn Lifespan Informatics and Neuroimaging Center, University of Pennsylvania, Philadelphia, PA 19104, USA
[8]Department of Psychiatry, University of Pennsylvania, Philadelphia, PA 19104, USA
[#]Co-first author
[*]Correspondence: cuizaixu@cibr.ac.cn

Abstract

The human cerebral cortex is connected by intricate inter-areal wiring at the macroscale. The cortical hierarchy from primary sensorimotor to higher-order association areas is a unifying organizational principle across various neurobiological properties; however, previous studies have not clarified whether the connections between cortical regions exhibit a similar hierarchical pattern. Here, we identify a connectional hierarchy indexed by inter-individual variability of functional connectivity edges, which continuously progresses along a hierarchical gradient from within-network connections to between-network edges connecting sensorimotor and association networks. We found that this connectional hierarchy of variability aligns with both hemodynamic and electromagnetic connectivity strength and is constrained by structural connectivity strength. Moreover, the patterning of connectional hierarchy is related to inter-regional similarity in transcriptional and neurotransmitter receptor profiles. Using the Neurosynth cognitive atlas and cortical vulnerability maps in 13 brain disorders, we found that the connectional hierarchy of variability is associated with similarity networks of cognitive relevance and that of disorder vulnerability. Finally, we found that the prominence of this hierarchical gradient of connectivity variability declines during youth. Together, our results reveal a novel hierarchal organizational principle at the connectional level that links multimodal and multiscale human connectomes to individual variability in functional connectivity.

Introduction

Functional brain connectivity exhibits organizational differences between individuals that are associated with individual differences in cognition and behavior[1-3]. Such inter-individual variability in regional functional connectivity is heterogeneously distributed across the cerebral cortex, exhibiting the lowest variability in primary sensorimotor cortices and maximum variability in higher-order association cortices[2,4,5]. This organizational pattern aligns with a macroscale cortical hierarchy arranged from primary sensorimotor to higher-order association cortices, with individual variability systematically increasing in a spatially continuous manner along this hierarchy[2,6]. However, existing studies were limited to the examination of hierarchical organization in the variability of regional functional connectivity, defined as a summarization of connection strength from one region to all other regions, and the organizing principle behind the variability of edge-level functional connectivity across the connectome remains unclear.

The human connectome is comprised of a complex network of inter-areal connections, which provide support to the dynamical communication between brain regions; this inter-regional communication can be represented as edge-level functional connections[7,8]. Variability in edge-level functional connections is correlated with cognition and behavior[1,9], and abnormalities in edge-level functional connectivity are associated with a wide range of psychiatric and neurological disorders[10,11]. Moreover, recent studies have demonstrated that edge-level functional connectivity partially explains the propagation of neurostimulation-induced signals across the brain; understanding variability in this connectivity could thus help to identify personalized stimulation targets[12,13]. Accordingly, understanding the spatial patterning of, and organizing principles behind, individual variability of edge-level functional connections has cognitive and clinical relevance.

Previous studies have identified the presence of individual variability in edge-level functional connectivity[14,15]. However, these studies did not examine the organizing principles for edge-level variability. Moreover, the underlying structural and molecular basis of edge-level functional variability as well as its implications in cognition, brain disorders and development have not been systematically investigated. Recent studies examining organizing principles governing other cortical features have demonstrated that many properties, including anatomical, functional, evolutionary, metabolic, molecular, and cognitive properties, exhibit concerted spatial variation along a unified large-scale cortical hierarchy[3,4,6,16-33], which aligned with the cortical distribution of individual variability. Here, we hypothesized a convergent hierarchical organization at the connectional level encompassing both the connectome of edge-level individual variability and a variety of multi-modal and multi-scale neurobiological connectomes in humans.

In this study, we identified the "connectional hierarchy" of the human connectome by analyzing inter-individual variability of functional connectivity at the edge level. We found that connectional hierarchy shows a continuous gradient from within-network connections along an axis towards between-network edges connecting sensorimotor and association networks. We observed that this connectional hierarchy aligns with both the hemodynamic functional network and multiple band-specific electromagnetic networks. Moreover, the connectional hierarchy of individual variability was constrained by the structural network, correlated gene expression network, and the network of neurotransmitter receptor expression. We also found that connectional hierarchy is associated with the network of cognitive relevance and that of disorder vulnerability. Finally, we demonstrated that connectional hierarchy evolves in youth towards more uniform individual variability across the connectome edges. Overall, we identified a novel connectional

hierarchy of individual functional variability, which is found to be a convergent organizing principle across multi-modal and multi-scale human connectomes.

Results

We harnessed two independent datasets, namely, the Human Connectome Project (HCP)-development (HCP-D, n = 415, 179 males, aged 8-21 years)[34] and unrelated HCP-young adults (HCP-YA, n = 245, 114 males, aged 22-35 years)[35] datasets, to estimate inter-subject variability of functional connectivity. To this end, we included 45- and 58-min blood oxygen level-dependent (BOLD) functional MRI data from the HCP-D and HCP-YA datasets, respectively. For each participant, we calculated the functional connectivity between every pair of cortical regions defined by an a priori Schaefer cortical parcellation atlas with 400 regions[36]. Functional connectivity was determined by the Pearson correlation coefficients between each pair of regional time series, resulting in a 400×400 symmetrical functional connectivity matrix for each participant. The matrix included 79,800 unique elements, and we denote each element as an "edge" between two cortical regions. We used a linear mixed-effects model to estimate both the inter-individual variability and intra-individual variability of each functional connectivity edge across all participants[39]. We scaled the inter-individual variability matrix by dividing by intra-individual variability to control for within-subject variation. This scaling also controls for the effect of functional connectivity strength over inter-individual variability as connectivity strength has a similar impact as the intra-individual variability which was divided by. Finally, a 400×400 symmetrical inter-individual variability matrix was generated, with each element representing the individual variation in the connectivity strength of this edge across all participants. We grouped the 400 cortical regions into networks according to the Yeo atlas[37], which consists of visual,

somatomotor, dorsal attention, ventral attention, frontoparietal, default mode, and limbic networks. The limbic network was excluded from subsequent analysis due to substantial signal loss (i.e., low signal to noise), especially in the orbitofrontal and ventral temporal cortex[3,19,38]. As a result, 374 cortical regions and 69,751 unique edges were finally analyzed in this study.

Individual variability gradually decreases along a connectional hierarchy from within-network to between-network edges

We generated individual variability matrices of functional connectivity for both the HCP-D (**Fig. 1a**) and HCP-YA (**Fig. 1b**) datasets. Visual inspection suggested that individual variability was heterogeneously distributed across all connectivity edges in both datasets, with the highest variability observed in within-network connections but not between-network connections. Specifically, high connectivity variability was prevalent in within-networks connections for the association networks, including default mode, frontoparietal, ventral, and dorsal attention networks, as well as within visual and somatomotor networks (though to a lesser extent). In contrast, we observed lower individual variability at between-network edges bridging association and sensorimotor regions. We found a significant correlation (Spearman's rho = 0.873, $P_{perm} < 0.001$, CI = [0.871, 0.875], two-sided) between individual variability of the HCP-YA and HCP-D datasets across all edges (**Fig. 1c**), indicating a highly stable distribution pattern of edge-wise individual variability. Spearman's rank correlation is applied to evaluate the similarity since the individual variability is not normally distributed.

Next, we summarized the network-level average individual variability, generating 6×6 matrices of within and between networks variabilities in the HCP-D (**Fig. 1d**) and HCP-YA (**Fig. 1e**) datasets. We observed that individual variability declined along a hierarchical axis from within-network connections to between-network connections. Taking the default mode network as

an example, individual variability declined along an axis progressing from edges within the default mode network to edges between default mode and other association networks, and continued to decrease at edges between the default mode and sensorimotor networks. A similar hierarchical pattern was observed for other higher-order association networks, including frontoparietal, ventral attention and dorsal attention networks. We refer to these hierarchical axes of individual variability as a "connectional hierarchy". These hierarchical axes of variability were highly consistent between the two independent datasets at the network level (Spearman's rho = 0.99, $P = 4.49\times10^{-6}$, CI = [0.96, 0.99], two-sided; **Fig. 1f**).

To explicitly visualize the connectional hierarchy, we ranked all the within-network and between-network variabilities for each network separately in both the HCP-D (**Fig. 1g**) and HCP-YA (**Fig. 1h**) datasets. We found that the ranking for each network was almost identical between HCP-D and HCP-YA, suggesting the robustness and reproducibility of the connectional hierarchy. The ranking indicated that for each network, individual variability declined from within-network connections to between-network edges connecting sensorimotor and association networks along a continuous gradient. The ranking also confirmed our observation that the variability declined along the within-network connections to connections between different association networks, and continuous to decline in sensorimotor-association network connections for each association network (**Fig.1g** and **Fig.1h**).

Having found a connectional hierarchical axis repeatedly for each association network, we examined the hierarchy of edge-level variability at a whole-brain connectome level. To do this, we ordered the individual variability of all the 21 network-level connections comprising both within-network and between-network connections rather than ordering each network separately (**Fig. S1**). The connections within association networks sit at the peak of this hierarchy, while the between-

network edges connecting sensorimotor and other networks were at the bottom end of the hierarchy. The variabilities of the six within-network connections and that of the six connections between association networks were higher than the variabilities of the nine connections between sensorimotor and other networks for both datasets.

Next, we assigned all connections to three groups, including within association networks (A-A), within sensorimotor networks (S-S), and between association and sensorimotor networks (S-A). A permutation test with 10,000 iterations was performed to test group differences. We found that the individual variability of A-A connections was significantly higher than that of S-A connections as well as that of S-S connections ($P_{perm} < 0.0001$) in both the HCP-D (**Fig. 1i**) and HCP-YA (**Fig. 1j**) datasets. Furthermore, S-S connections also displayed significantly higher variability than S-A connections ($P_{perm} < 0.0001$) in both datasets.

Overall, we found that for each of the six large-scale functional networks, the individual variability of within-network connections is generally higher than that of between-network connections. Moreover, for each higher-order association network, we observed a connectional hierarchical gradient from within-network connections to between-network connections, along which the individual variability continuously declines. Finally, we observed a boundary between connections within association networks and connections between association and sensorimotor networks.

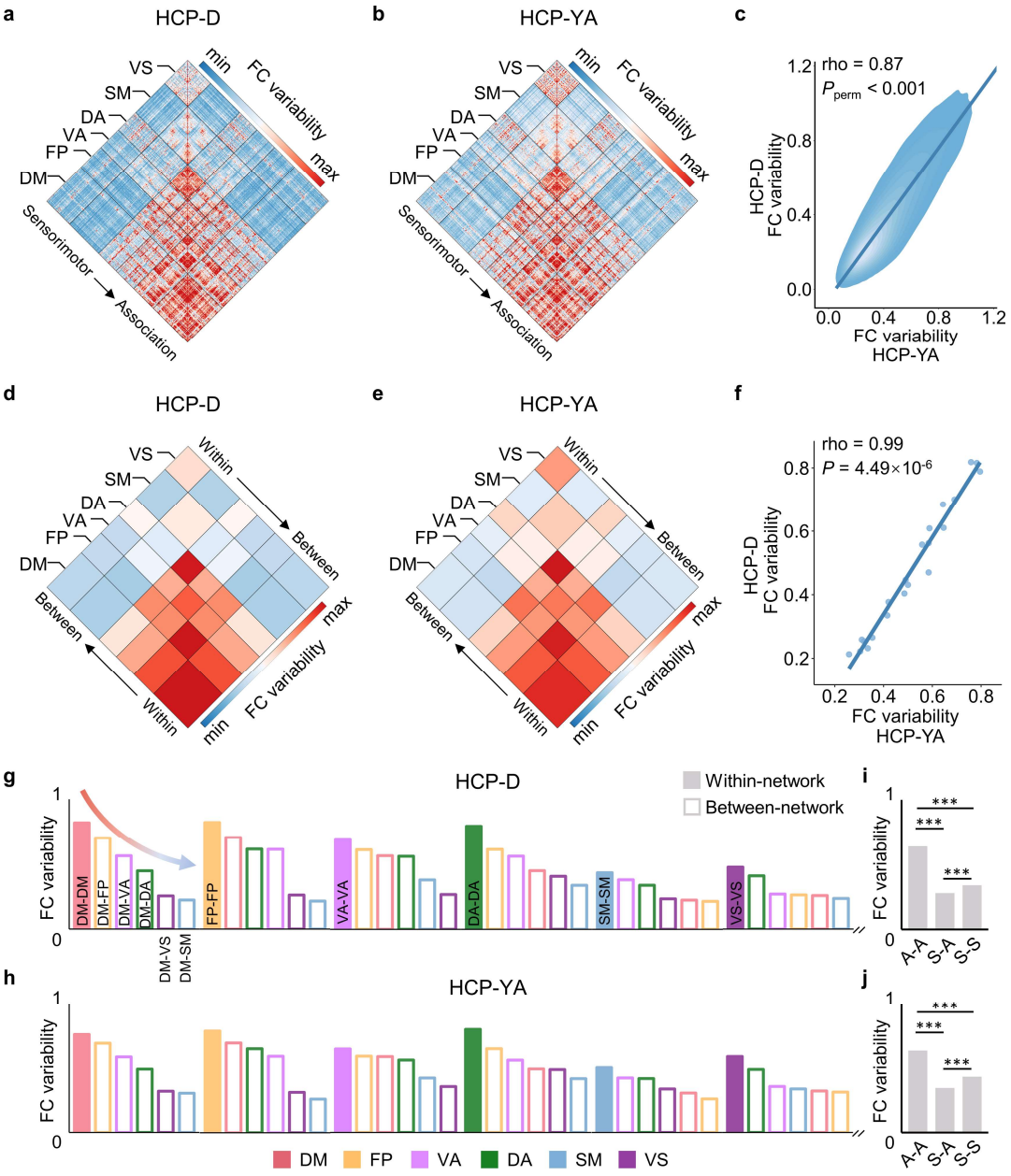

Fig. 1. Individual variability in edge-wise functional connectivity reveals the connectional hierarchy in the human brain. a, Inter-individual variability in functional connectivity across all participants in the HCP-D dataset. Variability was heterogeneously distributed across the connectivity edges. **b**, Inter-individual variability of functional connectivity in the HCP-YA dataset. **c**, Spearman's rank correlation coefficient showed that the individual variability was highly correlated (Spearman's rho = 0.873, $P_{perm} < 0.001$, CI = [0.871, 0.875], two-sided) between the HCP-D and HCP-YA datasets across all edges. **d**, **e**, Network-level average individual variability indicates that for each association network, the connectivity variability continuously declines along a hierarchical axis from within-network edges to between-network edges for both the HCP-D (**d**) and HCP-YA (**e**) datasets. **f**, Network-level average individual variability shows a high correlation between the HCP-D and HCP-YA datasets (Spearman's rho = 0.99, $P = 4.49\times10^{-}$

^{6}, CI = [0.96, 0.99], two-sided). **g**, **h**, Bar plots show the connectional hierarchy in the HCP-D (**g**) and HCP-YA (**h**) datasets. For each network, individual variability declines from within-network to between-network edges along a continuous gradient. **i**, **j**, Edge-wise individual variability within association networks (A-A) was significantly higher than that within sensorimotor networks (S-S) and that between sensorimotor and association networks (S-A), in both HCP-D (**i**) and HCP-YA (**j**) datasets. Additionally, S-S connections also exhibit higher variability than that of S-A in both datasets. A permutation test with 10,000 iterations was applied. *** indicates $P_{perm} < 0.0001$. FC, functional connectivity; VS, visual; SM, somatomotor; DA, dorsal attention; VA, ventral attention; FP, frontoparietal; DM, default mode.

Connectional hierarchy aligns with functional connectome characterized by synchronization of hemodynamic and band-specific electromagnetic activities

The functional connectome, as an intrinsic architecture of the brain, is characterized by specific spatial patterns and organizational principles. As the connectional hierarchy of individual variability defined in this study was derived from functional connectivity, we next examined to what degree connectional hierarchy aligns with functional connectivity per se. Thus, we averaged the BOLD functional connectivity matrices across participants and sessions within each dataset (**Fig. 2a**) and evaluated the association between functional connectivity and individual variability with Spearman's rank correlation. We found that the connectional hierarchy of individual variability was significantly correlated with BOLD functional connectivity in both the HCP-D (Spearman's rho = 0.47, $P_{perm} < 0.001$, CI = [0.47, 0.48], two-sided; **Fig. 2b**) and HCP-YA (Spearman's rho = 0.45, $P_{perm} < 0.001$, CI = [0.44, 0.46], two-sided; **Fig. 2c**). This result suggested that the connectional hierarchy in individual variability partially aligned with the pattern of the functional connectivity strength, with stronger functional connections being more variable across individuals. It should be noted that we already have controlled for the numeric impact of functional connectivity strength in inter-individual variability by dividing it using intra-individual variability.

Having identified that the connectional hierarchy of individual variability aligns with functional connectivity strength derived from BOLD fMRI, which measures the functional

synchronization at an infralow frequency (0.01-0.08 Hz), we are interested in how the organization of connectional hierarchy in individual variability associated with neural oscillation at different frequency bands. To do this, we examined the alignment between the connectional hierarchy of individual variability and electromagnetic functional connectivity from magnetoencephalography (MEG) data. We obtained resting-state MEG data from 36 unrelated healthy young adults (20 males, aged 22-35 years) in the HCP dataset. We extracted regional MEG time series with the Schaefer atlas at six frequency bands: delta (2 to 4 Hz), theta (5 to 7 Hz), alpha (8 to 12 Hz), beta (13 to 29 Hz), low-gamma (30 to 59 Hz), and high-gamma (60 to 90 Hz), similar to the approach employed in a prior study[40]. We then assessed the electromagnetic functional connectivity between each of the two regional time series using amplitude envelope correlation and averaged the functional connectivity matrices across all participants for each frequency band (**Fig. 2d**).

Visual examination indicated that MEG functional connectivity was heterogeneously distributed across all connectivity edges at each frequency band. We compared the six MEG functional connectivity matrices (**Fig. 2d**) with the individual variability matrices (**Fig. 1a** and **1b**) from both the HCP-D and HCP-YA datasets. Connectional hierarchy in individual variability was correlated with MEG functional connectivity across all edges at multiple frequency bands in both the HCP-D (2-4 Hz: Spearman's rho = 0.36; 5-7 Hz: rho = 0.19; 8-12 Hz: rho = 0.06; 13-29 Hz: rho = 0.32; 30-59 Hz: rho = 0.22; 60-90 Hz: rho = 0.15; all Bonferroni-corrected $P_{perm} < 0.001$, except for alpha) and HCP-YA (2-4 Hz: rho = 0.33; 5-7 Hz: rho = 0.26; 8-12 Hz: rho = 0.13; 13-29 Hz: rho = 0.34; 30-59 Hz: rho = 0.14; 60-90 Hz: rho = 0.04; all Bonferroni-corrected, $P_{perm} < 0.005$, except for high-gamma) datasets (**Fig. 2e**). The correlations were higher at the delta and beta frequency bands (rho > 0.3 in both datasets) and relatively lower for theta, alpha, low-gamma, and high-gamma frequency bands. These results suggest that the pattern of connectional hierarchy

is significantly associated with the synchronization of electrophysiological oscillations at specific frequency bands.

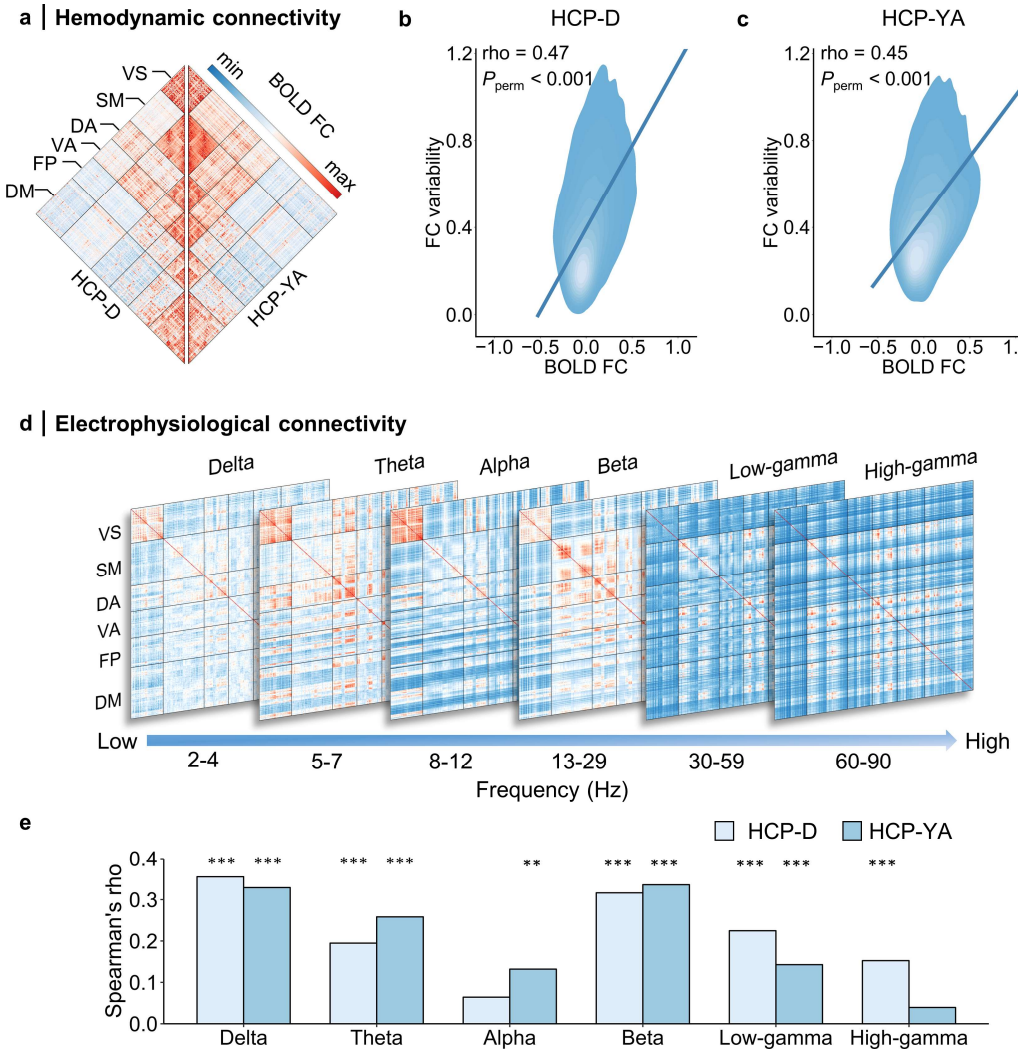

Fig. 2. Hemodynamic and electrophysiological functional connectome basis of connectional hierarchy. a, The group-averaged functional connectivity matrices from BOLD fMRI data for both HCP-D (left half matrix) and HCP-YA (right half matrix) datasets. **b**, **c**, Individual variability in functional connectivity was positively correlated with BOLD functional connectivity strength across all edges in both HCP-D (**f**, Spearman's rho = 0.47, $P_{perm} < 0.001$, CI = [0.47, 0.48], two-sided) and HCP-YA (**g**, Spearman's rho = 0.45, $P_{perm} < 0.001$, CI = [0.44, 0.46], two-sided) datasets. **d**, Group-averaged functional connectivity matrices obtained using MEG data of 36 unrelated healthy young adult participants from the HCP dataset. MEG connectivity was estimated at six bands, including delta (2 to 4 Hz), theta (5 to 7 Hz), alpha (8 to 12 Hz), beta (13 to 29 Hz), low-gamma (30 to 59 Hz), and high-gamma (60 to 90 Hz). **e**, The association between individual variability (from **Fig. 1a** and **Fig. 1b**) and MEG connectivity across all network edges at six frequency bands for both datasets was determined using Spearman's rank correlation. HCP-D

dataset: 2-4 Hz: rho = 0.36; 5-7 Hz: rho = 0.19; 8-12 Hz: rho = 0.06; 13-29 Hz: rho = 0.32; 30-59 Hz: rho = 0.22; 60-90 Hz: rho = 0.15. HCP-YA dataset: 2-4 Hz: rho = 0.33; 5-7 Hz: rho = 0.26; 8-12 Hz: rho = 0.13; 13-29 Hz: rho = 0.34; 30-59 Hz: rho = 0.14; 60-90 Hz: rho = 0.04. The Spearman's rank correlation was used, two-sided. *** indicates $P_{perm} < 0.001$, ** indicates $P_{perm} < 0.005$, Bonferroni-corrected.

Connectional hierarchy is constrained by the structural connectome

Having demonstrated the connectional hierarchy in individual variability aligned with both the hemodynamic and multiple band-specific electromagnetic connectivity, we sought to understand the structural basis of the connectional hierarchy of individual variability. Previous studies have reported that structural connectivity constrains the dynamic communication between cortical regions and shapes the pattern of functional connectivity[41,42]. We hypothesized that the pattern of the structural connectome is associated with the organization in individual functional variability. Using diffusion MRI datasets, we reconstructed the whole-brain white matter tracts of individual participants using a probabilistic fiber tractography with multi-shell multi-tissue constrained spherical deconvolution[43]. The anatomically constrained tractography (ACT)[44] and spherical-deconvolution informed filtering of tractograms (SIFT)[45] were applied to improve the biological accuracy of fiber reconstruction (See **Methods**). We counted the number of streamlines between each of the two cortical regions defined by the Schaefer atlas, resulting in a 374×374 structural network of streamline counts for each participant (**Fig. 3a**). The connection strength was normalized by dividing the average volume of the two regions, and was then log-transformed. Next, we averaged structural networks across all participants for the HCP-D and HCP-YA datasets (**Fig. 3a**).

Structural connectivity is heterogeneously distributed across network edges, with dense connections within networks and sparse connections between networks. We showed the upper triangle of the structural network and individual variability matrix side-by-side for both the HCP-

D (**Fig. 3b**) and HCP-YA (**Fig. 3c**) datasets, which share a similar pattern, especially in terms of the higher connection strength at the edges both within and between association networks. The sum of network-level average values indicated an overall similar pattern between structural network and individual variability across all edges for both datasets (**Fig. 3d** and **Fig. 3e**). We observed a similar connectional hierarchical axis for higher-order association networks as individual variability. For example, the structural connectivity decline from the connections within default mode network to the connections between default mode network and other association networks, and continuously declines to the connections between default mode network and sensorimotor networks. Finally, we found a significant correlation between individual variability and structural connectivity across all edges with non-zero structural connectivity for both the HCP-D (Spearman's rho = 0.24, $P_{perm} < 0.001$, CI = [0.23, 0.26], two-sided; **Fig. 3f**) and HCP-YA (Spearman's rho = 0.26, $P_{perm} < 0.001$, CI = [0.25, 0.28], two-sided; **Fig. 3g**) datasets, indicating that an edge with a higher structural connection strength also shows higher individual variability in functional connectivity. Overall, these results suggest that the structural connectome constrains the pattern of connectional hierarchy in individual variability.

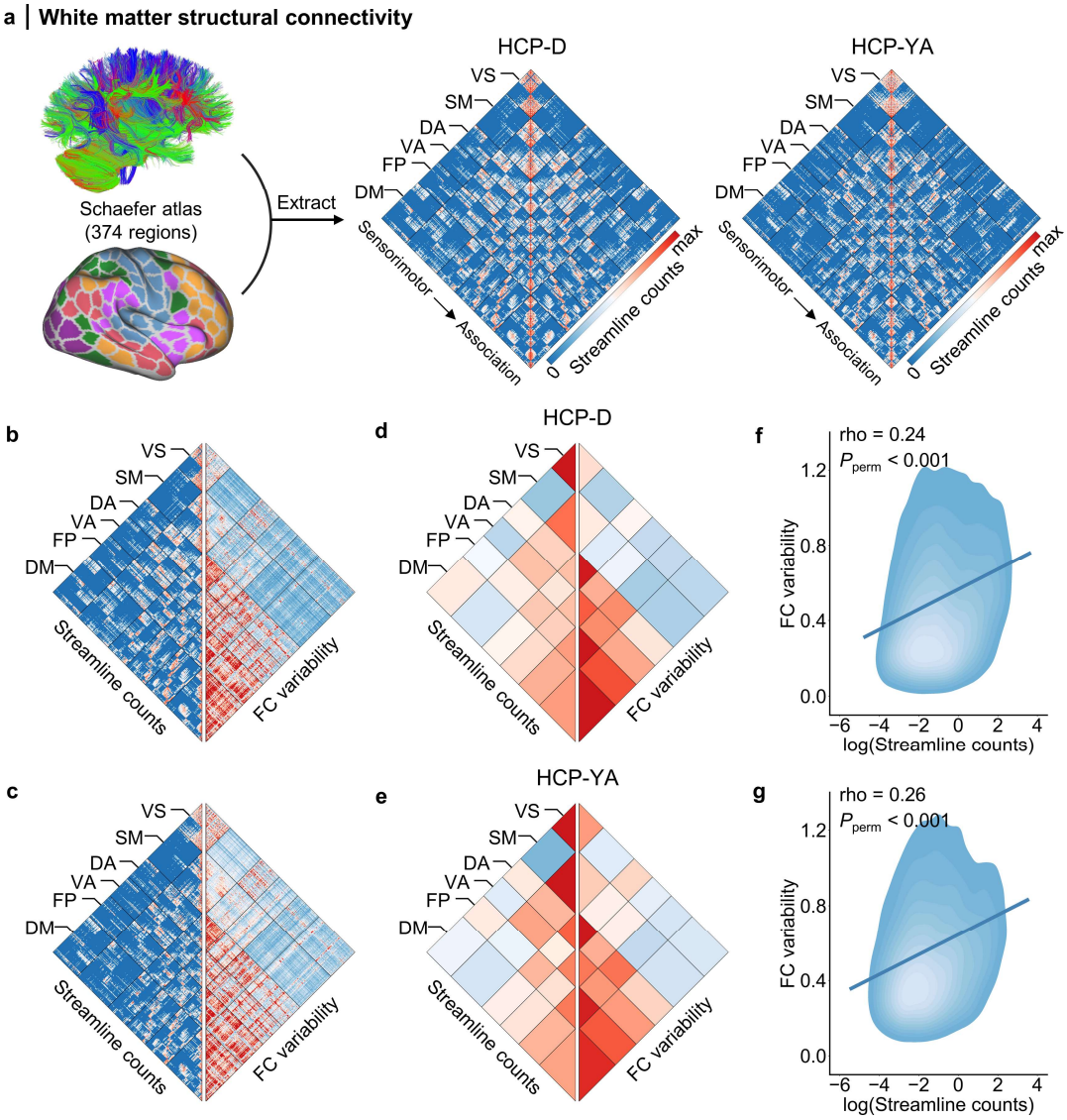

Fig. 3. Structural connectome basis of connectional hierarchy in FC variability. a, The structural network was constructed based on white matter tracts tractography from diffusion MRI data and the Schaefer atlas. Edge strengths in the structural network indicate the white matter fiber density between pairs of regions. The connection strength was log-transformed. **b**, **c**, Side-by-side comparison of structural connectivity and individual FC variability matrices in the HCP-D (**b**) and HCP-YA (**c**) datasets. **d**, **e**, Network-level average of structural connectivity and individual FC variability in HCP-D (**d**) and HCP-YA (**e**) datasets. **f**, **g**, Individual FC variability was positively correlated with structural connectivity strength across all edges in both HCP-D (**f**, Spearman's rho = 0.24, $P_{perm} < 0.001$, CI = [0.23, 0.26], two-sided) and HCP-YA (**g**, Spearman's rho = 0.26, $P_{perm} < 0.001$, CI = [0.25, 0.28], two-sided) datasets. FC, functional connectivity.

Connectional hierarchy is shaped by a correlated gene expression network as well as a network of neurotransmitter receptor expression

Having demonstrated that structural connectivity might scaffold the connectional hierarchy of individual variability, we investigated the molecular mechanisms supporting connectional hierarchy. The correlated gene expression network, defined by the correlation of transcriptional profiles between pairs of cortical regions across genes, has been shown to be associated with the synchronization of functional activities[46-48]. Therefore, we hypothesized that the pattern of the correlated gene expression network would associate with the connectional hierarchy of individual functional variability.

To test this hypothesis, we acquired gene expression data from the Allen Human Brain Atlas (AHBA, http://human.brain-map.org)[49], a transcriptional atlas sampled from hundreds of brain samples using DNA microarray probes in six human postmortem brains (5 males; age, 24-57 years). Using the approach described in previous studies[16,22,47,48], we calculated the group-averaged gene transcriptional profiles of all 2,256 selected brain-specific genes for each cortical region in the Schaefer atlas (**Fig. 4a**). We then estimated the correlated gene expression network for all genes using Pearson correlation coefficients of the transcriptional profiles between every two cortical regions. A side-by-side comparison of the correlated gene expression network from the AHBA dataset and the individual variability network from BOLD fMRI suggests a similar pattern of connectional hierarchy from within-network to between-network connections for both HCP-D (**Fig. 4b**) and HCP-YA (**Fig. 4c**) datasets. Network-level average values of gene expression and FC variability confirmed their similarity across all network edges in both datasets (**Fig. 4d** and **Fig. 4e**). To quantify this observation, we found a significant correlation between the correlated gene expression network and the individual variability across all the network edges for both the HCP-D (Spearman's rho = 0.29, $P_{perm} < 0.001$, CI = [0.28, 0.30], two-sided; **Fig. 4f**) and HCP-YA

(Spearman's rho = 0.37, $P_{perm} < 0.001$, CI = [0.37, 0.38], two-sided; **Fig. 4g**) datasets. These results suggest that the connectional hierarchy is rooted in the transcriptional profiles of gene expression.

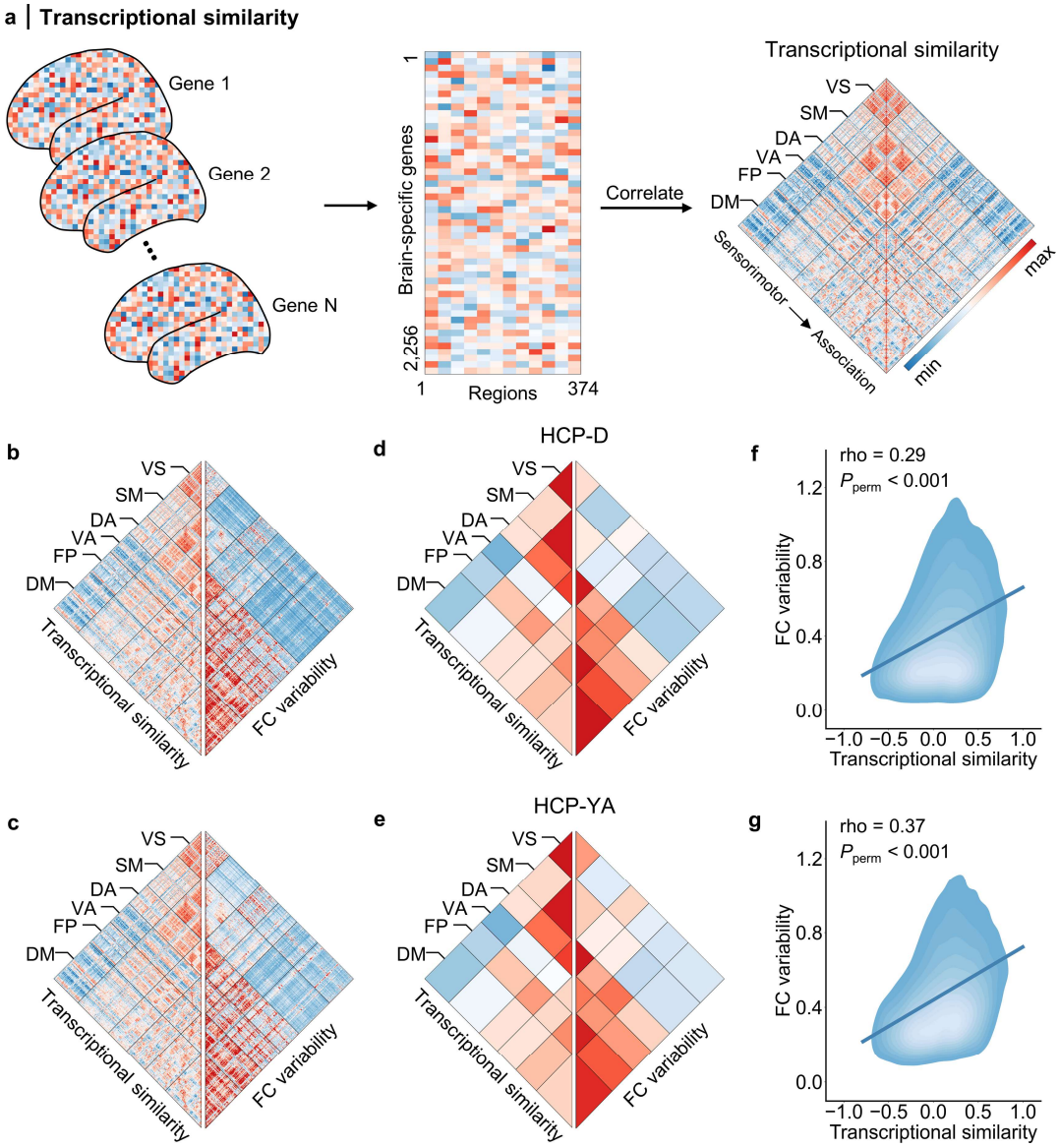

Fig. 4. Transcriptional similarity of gene expression underlying connectional hierarchy. a, The workflow to construct a correlated gene expression network. Gene expression data were acquired from the Allen Human Brain Atlas[49], and 2,256 brain-specific genes were selected. The group transcriptional profiles across all genes were extracted for each cortical region according to the Schaefer atlas, yielding a 374×2,256 region×gene matrix. The correlated gene expression network was measured by determining the Pearson correlation coefficients of transcriptional profiles between pairs of cortical regions. **b**, **c**, Side-by-side comparison between the correlated gene expression network and individual variability network in both HCP-D (**b**) and HCP-YA (**c**) datasets. **d**, **e**, Network-level average of transcriptional similarity and individual FC variability in

the HCP-D (**d**) and HCP-YA (**e**) datasets. **f**, **g**, The individual FC variability was positively correlated with transcriptional similarity strength across all edges in both HCP-D (**f**, Spearman's rho = 0.29, $P_{perm} < 0.001$, CI = [0.28, 0.30], two-sided) and HCP-YA (**g**, Spearman's rho = 0.37, $P_{perm} < 0.001$, CI = [0.37, 0.38], two-sided) datasets. FC, functional connectivity.

Neurotransmitter receptors and transporters support the propagation of electrical impulses and shape the synchronization of neural activity[27]. We hypothesized an association between the expression of neurotransmitter receptors and transporters and the connectional hierarchy in individual functional variability. For this assessment, we obtained the neurotransmitter receptor data from a prior study by Hansen et al.[27], which included the cortical distribution maps of 19 different neurotransmitter receptors and transporters from PET maps of more than 1200 participants. These data provide the regional average density of the 400 cortical regions in the Schaefer atlas for each of the 19 receptors and transporters. We calculated the Pearson correlation coefficients of the density between each of the two cortical regions across the 19 neurotransmitter receptors and transporters, resulting in a 374×374 matrix (without limbic network) of between-region similarity, called the receptor similarity network (**Fig. 5a**). We found that the receptor similarity network aligned with the individual variability map and that receptor similarity also declined along the hierarchy axis from within-network to between-network edges for both the HCP-D (**Fig. 5b**) and HCP-YA (**Fig. 5c**) datasets. Network-level average values of receptor similarity and individual variability confirmed their similarity across all network edges for both datasets (**Fig. 5d** and **Fig. 5e**). Using Spearman's rank correlations, we found that receptor similarity is positively correlated with FC variability across all network edges for both the HCP-D (Spearman's rho = 0.35, $P_{perm} < 0.001$, CI = [0.34, 0.35], two-sided; **Fig. 5f**) and the HCP-YA (Spearman's rho = 0.38, $P_{perm} < 0.001$, CI = [0.37, 0.38], two-sided; **Fig. 5g**) datasets. These results

suggest that the between-region similarity of the neurotransmitter receptor and transporter profiles is associated with the connectional hierarchy of individual variability.

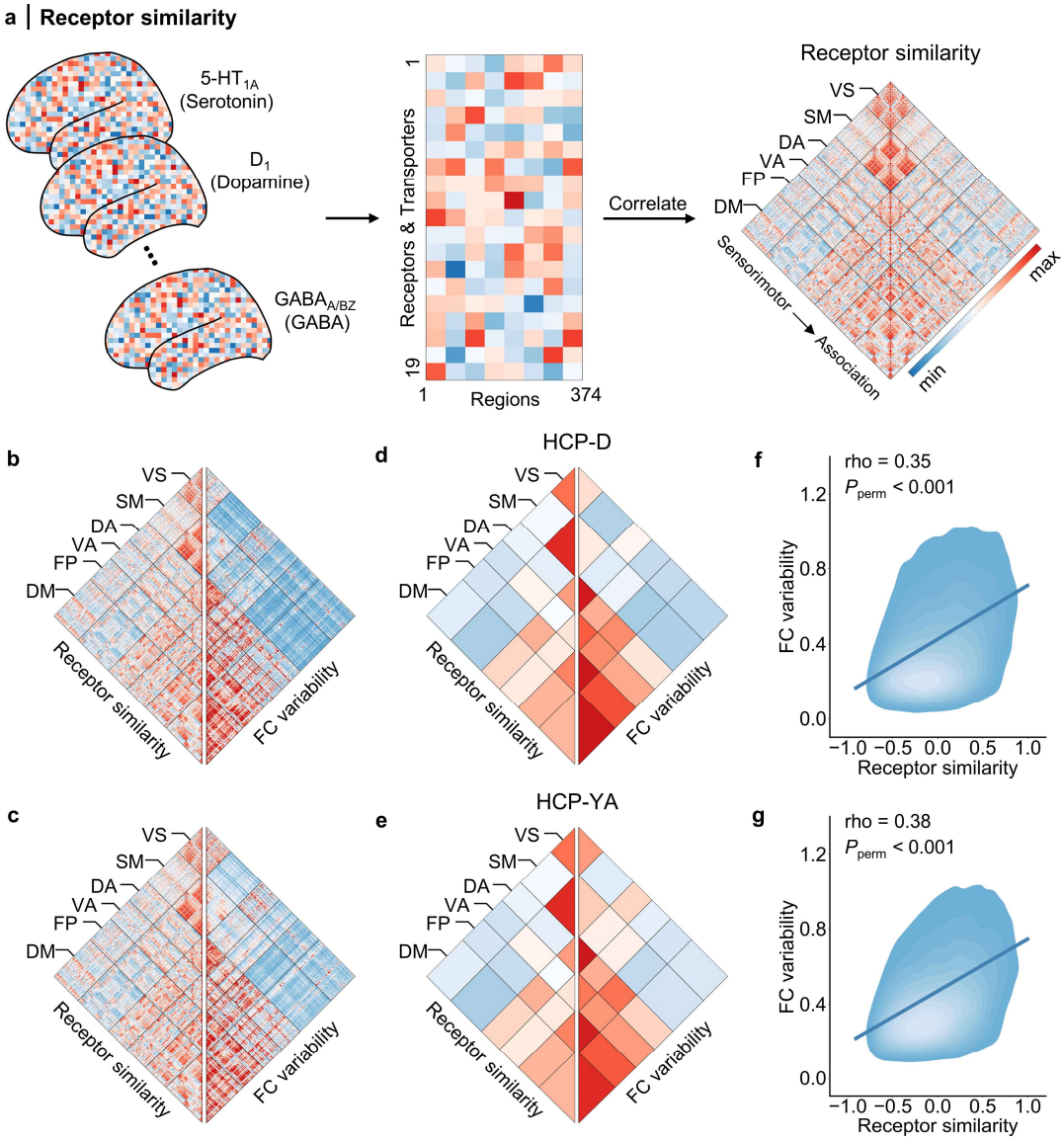

Fig. 5. Network of neurotransmitter receptor and transporter expression shapes connectional hierarchy. A, We obtained the distribution of 19 different neurotransmitter receptors and transporters in each of the 374 cortical regions defined with the Schaefer atlas from a prior study[27]. We calculated the Pearson correlation coefficients of the receptor and transporter densities between each pair of cortical regions, resulting in a 374×374 matrix of between-region similarity of neurotransmitter receptor and transporter expression. **b**, **c**, Side-by-side comparisons between receptor similarity and individual variability matrices in the HCP-D (**b**) and HCP-YA (**c**) datasets. **d**, **e**, Network-level average of receptor similarity and FC variability in the HCP-D (**d**) and HCP-YA (**e**) datasets. **f**, **g**, Individual FC variability was positively correlated with receptor similarity strength across all edges in both HCP-D (**f**, Spearman's rho = 0.35, $P_{perm} < 0.001$, CI =

[0.34, 0.35], two-sided) and HCP-YA (**g**, Spearman's rho = 0.38, $P_{perm} < 0.001$, CI = [0.37, 0.38], two-sided) datasets. FC, functional connectivity.

The implications of connectional hierarchy for cognition and brain disorders

Having demonstrated that the connectional hierarchy from individual variability is a convergent organizing principle that aligns with inter-regional functional, structural, and molecular networks, we hypothesized that connectional hierarchy could be implicated in human cognition and brain disorders. Therefore, we compared the alignment between connectional hierarchy and the network of regional cognitive relevance as well as the network of regional disorder vulnerability.

We estimated regional relevance to a variety of cognitive functions based on a prior study[22]. First, we acquired whole-brain activation probability maps of 123 cognitive terms from Neurosynth[50] and Cognitive Atlas[51]. Based on these data, we calculated the regional average activation probability of each cognitive term, resulting in a matrix with 374 rows (i.e., regions) and 123 columns (i.e., term), which reflects the activation probability of each cortical region associated with a specific type of cognition. Next, we calculated the Pearson correlation of activation probability between each pair of brain regions across all 123 terms, resulting in a 374×374 similarity matrix of between-region cognitive relevance (**Fig. 6a**). A side-by-side comparison indicated that the correlated network of regional cognitive relevance was highly similar to the connectional hierarchy in individual variability for both the HCP-D (**Fig. 6b**) and HCP-YA (**Fig. 6c**) datasets. Thus, the pairs of regions were initially associated with highly similar sets of cognitions and gradually transited to associate with different cognitions along the hierarchical axis from within-network to between-network edges. The pattern of network-level average values confirmed this similarity between the cognitive relevance network and individual

variability network in both datasets (**Fig. 6d** and **Fig. 6e**). Finally, we observed a correlation between the cognitive network and the individual variability network across all edges for both the HCP-D (Spearman's rho = 0.48, $P_{perm} < 0.001$, CI = [0.47, 0.49], two-sided; **Fig. 6f**) and HCP-YA (Spearman's rho = 0.46, $P_{perm} < 0.001$, CI = [0.45, 0.46], two-sided; **Fig. 6g**) datasets. Overall, these results suggest that connectional hierarchy reflects the regional similarity in cognitive relevance profiles.

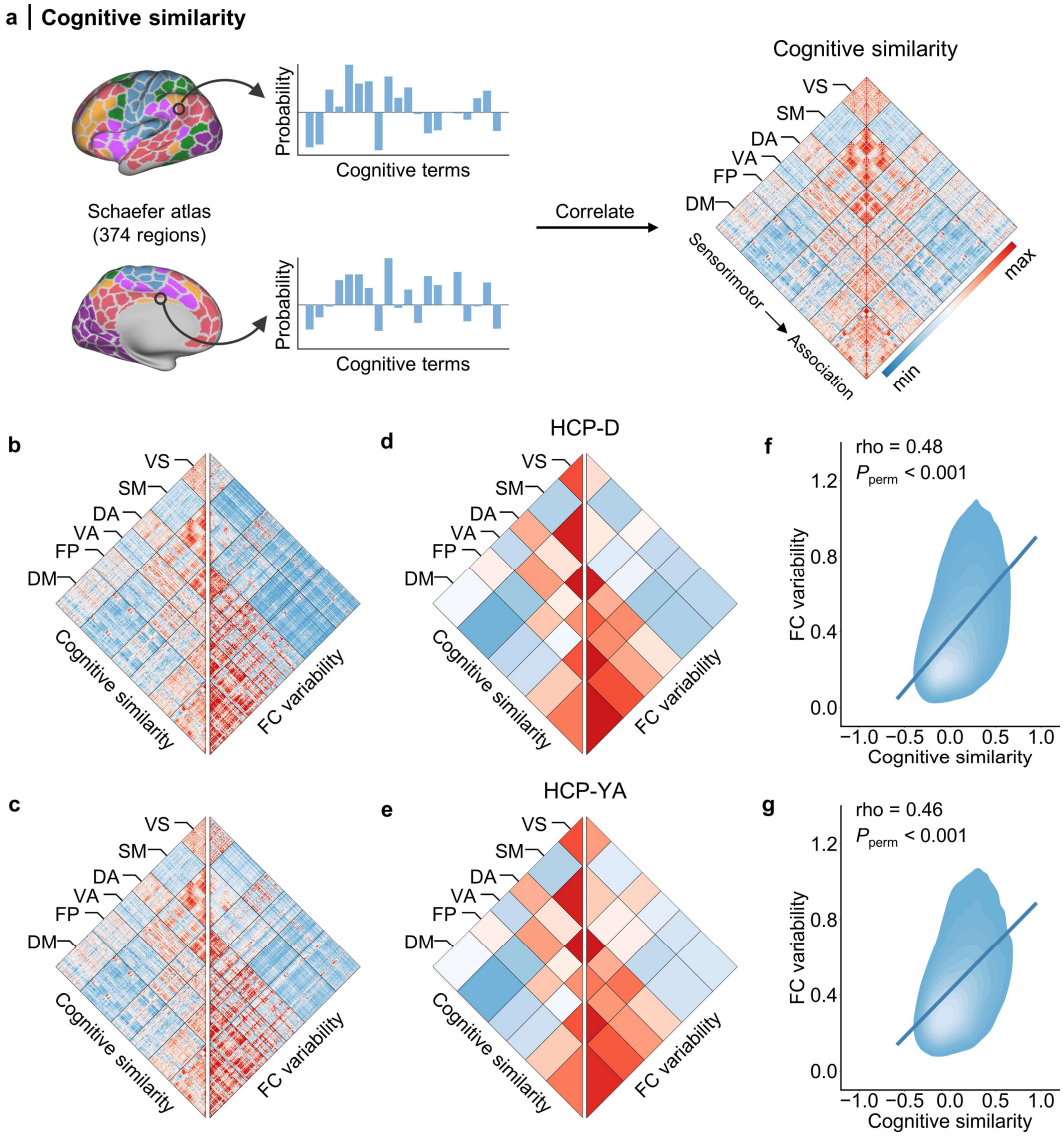

Fig. 6. Implications of connectional hierarchy in cognition. a, With data from Neurosynth[50] and Cognitive Atlas[51], we extracted the activation probability of 123 different cognitive terms in each

of the 374 cortical regions defined with the Schaefer atlas. We calculated the Pearson correlation of the activation probability profiles between every two cortical regions across 123 terms, resulting in a 374×374 matrix of between-region similarity of cognitive relevance. **b**, **c**, Side-by-side comparisons between the similarity network of cognitive relevance and individual FC variability matrices in the HCP-D (**b**) and HCP-YA (**c**) datasets. **d**, **e**, Network-level average of cognitive similarity and individual FC variability in the HCP-D (**d**) and HCP-YA (**e**) datasets. **f**, **g**, Individual FC variability was positively correlated with the similarity network of cognitive relevance across all edges in both HCP-D (**f**, Spearman's rho = 0.48, $P_{perm} < 0.001$, CI = [0.47, 0.49], two-sided) and HCP-YA (**g**, Spearman's rho = 0.46, $P_{perm} < 0.001$, CI = [0.45, 0.46], two-sided) datasets. FC, functional connectivity.

Next, we evaluated the implications of connectional hierarchy in brain disorders by examining the similarity between the pattern of connectional hierarchy and the network of disorder vulnerabilities. Based on literature[52], we acquired the cortical thickness abnormality maps of 13 different brain disorders from the ENIGMA consortium[53] by using the ENIGMA toolbox (https://enigma-toolbox.readthedocs.io/)[54]. These disorders included 22q11.2 deletion syndrome, attention deficit hyperactivity disorder, autism spectrum disorder, epilepsy (the idiopathic generalized, right temporal lobe, and left temporal lobe subtypes), depression, obsessive-compulsive disorder, schizophrenia, bipolar disorder, obesity, schizotypy, and Parkinson's disorders. The acquired data included the statistical values of cortical thickness abnormalities in 68 cortical regions, which were defined by the Desikan–Killiany atlas[55], for each disorder. We calculated the Pearson correlation coefficients for the regional statistical values of thickness abnormality between pairs of cortical regions across 123 disorders, resulting in a 68×68 network of correlated disorder vulnerability (**Fig. 7a**). For comparison with this network, we regenerated the individual variability of functional connectivity with 68 cortical regions for the HCP-D (**Fig. 7b**, left-half matrix) and HCP-YA (**Fig. 7b**, right-half matrix) datasets using the Desikan–Killany atlas. We did not label the Yeo networks on the matrices, since these 68 regions did not match well with the Yeo networks. Spearman's rank correlation analysis revealed that the disorder

vulnerability network was significantly correlated with the individual variability network in both the HCP-D (Spearman's rho = 0.30, $P_{perm} < 0.001$, CI = [0.26, 0.33], two-sided; **Fig. 7c**) and HCP-YA (Spearman's rho = 0.25, $P_{perm} < 0.001$, CI = [0.21, 0.29], two-sided; **Fig. 7d**) datasets. These results suggest that the pattern of connectional hierarchy shapes regional co-vulnerability to a variety of brain disorders.

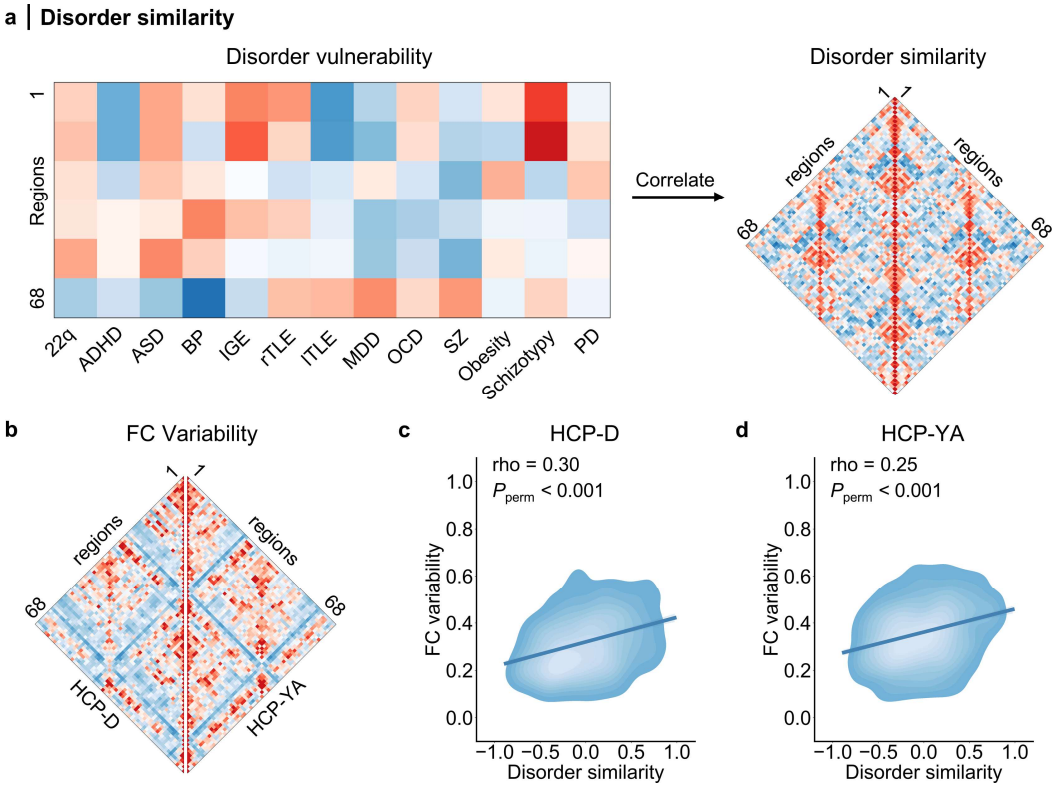

Fig. 7. Implications of connectional hierarchy for brain disorders. a, The cortical thickness abnormality maps for 13 neurological, neurodevelopmental, and psychiatric disorders were obtained from the ENIGMA consortium[53] with ENIGMA toolbox (https://enigma-toolbox.readthedocs.io/)[54]. We extracted the regional cortical abnormalities according to the Desikan–Killiany atlas with 68 cortical regions, and calculated the Pearson correlation coefficients of the disorder abnormality profiles between each pair of regions to construct the similarity network of disorder vulnerability. **b**, The matrices of individual variability in functional connectivity using the HCP-D (left half) and HCP-YA (right half) datasets. **c**, **d**, Individual FC variability was positively correlated with the network of disorder vulnerability across all edges in both HCP-D (**c**, Spearman's rho = 0.30, $P_{perm} < 0.001$, CI = [0.26, 0.33], two-sided) and HCP-YA (**d**, Spearman's rho = 0.25, $P_{perm} < 0.001$, CI = [0.21, 0.29], two-sided) datasets. FC, functional connectivity. 22q, 22q11.2 deletion syndrome; ADHD, attention-deficit/hyperactivity disorder; ASD, autism spectrum disorder; BP, bipolar disorder; IGE, idiopathic generalized epilepsy; rTLE,

right temporal lobe epilepsy; lTLE, left temporal lobe epilepsy; MDD, major depressive disorder; OCD, obsessive-compulsive disorder; SZ, schizophrenia; PD, Parkinson's disease.

Connectional hierarchy evolves in youth towards a more uniform individual variability across connectome edges

Finally, we investigated the maturation of the connectional hierarchy of individual variability in youth. Using the HCP-D dataset (8~21 years), we split the data into 14 groups, with each age year representing one group. We calculated an inter-individual variability matrix for each age group at the network level. According to a prior study[56], we quantitively defined the connectional hierarchy as the inter-edge heterogeneity of individual variability across the network level edges (**Fig. 8a**). Specifically, we calculated the inter-edge heterogeneity as the median absolute deviation (MAD) of the individual variability across the 21 network-level edges, including 6 within-network and 15 between-network edges. Using this approach, we calculated the inter-edge heterogeneity across network-level edges for each of the 14 groups. As in previous brain development studies[3,57-59], we used a general additive model (GAM)[60] to capture linear and nonlinear associations with age while controlling for sex and in-scanner motion. The results indicated that inter-edge heterogeneity significantly declined with age (Z = -2.34, P = 0.019, and partial r = -0.66, CI = [-0.88, -0.20], two-sided; **Fig. 8b**), suggesting the gradient of connectional hierarchy decreased to yield a more uniform profile of individual variability across connectome edges at older ages in youth.

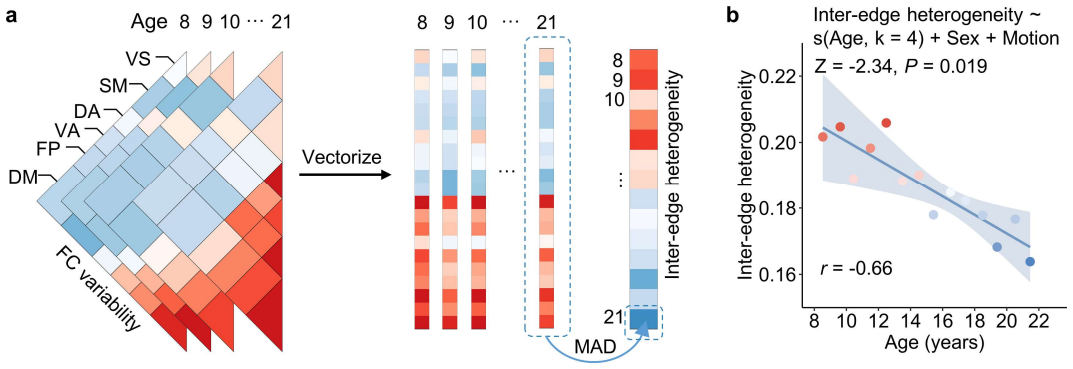

Fig. 8. Development of connectional hierarchy in youth. a, Quantification procedure of the connectional hierarchy as inter-edge heterogeneity in individual variability. Participants in the HCP-D dataset were split into 14 age groups (from 8 to 21 years) with an interval of one year. The individual variability of functional connectivity was computed independently for each group at the network level. The unique elements of the variability matrix were extracted as a vector, and the median absolute deviation (MAD) was computed as the inter-edge heterogeneity. **b**, Scatterplot of the relationship between age and the inter-edge heterogeneity. After controlling for sex and in-scanner motion, the general additive model (GAM) identified a significant negative association between inter-edge heterogeneity and age. FC, functional connectivity.

Sensitivity analyses

As prior studies demonstrated both structural and functional connectivity were associated with physical distance between regions[61,62], we examined the effects of interregional distance on our results. Prior studies have reported that cortical regions located nearby are likely to share analogous molecular and structural bases, which potentially support similar functions[27,61,63]. To minimize the effect of spatial proximity, we regressed out the Euclidean distance between regions from the individual variability matrix as well as other networks. The pattern of individual variability remains significantly correlated with all other networks (**Fig. S2-S4**), including hemodynamic connectivity (HCP-D: Spearman's rho = 0.47; HCP-YA: rho = 0.44), electromagnetic connectivity (delta: rho = 0.31; beta: rho = 0.28 for HCP-D; delta: rho = 0.29; beta: rho = 0.33 for HCP-YA), structural connectivity (HCP-D: rho = 0.21; HCP-YA: rho = 0.23), transcriptional similarity network (HCP-D: rho = 0.24; HCP-YA: rho = 0.34), neurotransmitter receptor network (HCP-D: rho = 0.32; HCP-YA: rho = 0.36), similarity network of cognitive

relevance (HCP-D: rho = 0.46; HCP-YA: rho = 0.43), and similarity network of disorder vulnerability (HCP-D: rho = 0.23; HCP-YA: r = 0.20). These results suggest that the convergent pattern of the connectional hierarchy across multiple scales was not driven by spatial proximity. Additionally, after controlling the effects of inter-regional distance in each of the fourteen age groups, we also observed a significant negative association between age and inter-edge heterogeneity (Z = -2.12, P = 0.034, and partial r = -0.61; **Fig. S5**).

Discussion

In this study, we identified a connectional hierarchy as a fundamental organizing principle of connectome edges by evaluating the inter-individual variability in edge-level functional connectivity. We found that this connectional hierarchy of individual variability progresses from within-network connections to the edges between sensorimotor and association networks along a continuous gradient. The connectional hierarchy aligns with both BOLD functional connectivity and multiple band-limited electromagnetic connectivity. We also found that such connectional hierarchy is constrained by structural connectivity and associates with the similarity network of gene expression as well as that of neurotransmitter receptor expression. Moreover, the connectional hierarchy of individual variability exhibits a similar organization as networks of cognitive relevance and disorder vulnerability. These results were highly consistent across two independent datasets and are robust after controlling for between-region distances. Finally, we found that the connectional hierarchy of individual variability evolves in youth towards a more uniform pattern. Overall, we reveal a fundamental organizing principle at the connectome edge level, which links various neurobiological properties and relates to cognition, brain disorders, and human development.

Prior studies have found that individual variability of functional connectivity is heterogeneously distributed across the cortex with a maximum variability in the association cortex and a gradual decrease along an axis towards the sensorimotor cortex[2,5]. This organization of variability follows the pattern of cortical hierarchy, which is a principal axis spatially progressing from the primary sensorimotor cortices to higher-order association cortices that support advanced mental functions[4,6,21]. Building on these studies, our findings provided a novel connectional hierarchy, which describes the distribution of individual variability of functional connectivity across the connectome edges. By examining the edges connected to each network separately, or, alternatively, ordering all the network-level edges across the whole connectome, we consistently observed the connectional hierarchy as a continuous gradient along which individual variability declines from within-network connections to connections between sensorimotor and association networks. Such a pattern of connectional hierarchy is highly consistent between the two independent datasets.

Cortical hierarchy that spans from sensorimotor to association cortices has been identified as a unifying organizing principle of the human cerebral cortex[2-4,6,16-31,33]. This pattern has been observed in the cortical distribution of a variety of fundamental properties, such as neuron density and myelin content[16,25,64], functional spatiotemporal variance[2,3,18,19,23], metabolism[20,58], and gene expression[16]. Similarly, we found that the connectional hierarchy, which progresses from within-network connections along a continuous gradient towards the edges between sensorimotor and association networks, serves as a convergent organizing principle across multi-modal and multi-scale human connectomes. We observed that this hierarchy is evident in functional, structural, and molecular connectomes, as well as in the connectomes for cognitive relevance and disorder vulnerability.

We found that both the hemodynamic functional connectivity and the electromagnetic connectivity[40] at the delta and beta frequency bands display higher connection strengths for within-networks connections, and gradually declines along the connectional hierarchy towards the edges between sensorimotor and association networks. Moreover, anatomical white matter tracts are denser within networks and become progressively sparse down the axis of the connectional hierarchy. This result aligns with conclusions from previous literature that macroscale anatomical connectivity supports functional dynamics[41,42]. This hierarchical axis is also observed in molecular networks. Specifically, the between-regional similarities in both transcription and receptor density maps continuously decline along the connectional hierarchy from within-network connections to sensorimotor-association connections. These results are further confirmed by prior work explaining that gene expression profiles[46,48] and neurotransmitter receptor profiles[27] shape the synchronization of brain networks. In summary, we demonstrated that the connectional hierarchy of individual variability is a unifying organizing principle across multiple neurobiological connectomes in humans. Our conclusions are further supported by a recent preprint suggesting a convergent network topological organization across these multi-modal and multi-scale human connectomes[65]. Looking beyond the scope of this prior study[65], our work provides a systematic characterization of the hierarchical organization across the connectome edges.

Importantly, we found the axis of connectional hierarchy is relevant to both cognition and brain disorders. Prior work has reported that the cortical distribution of cognition and behavior aligned with the cortical hierarchy of individual functional variability[2]. Here, we further demonstrated that the connectome of cognitive relevance, quantified as the inter-regional network of activation pattern similarity across 123 cognitive terms[22,50], is organized along the connectional hierarchical gradient. Additionally, while it has been shown that brain regions with similar

molecular, structural, or functional profiles are affected similarly across disorders[52], here we posit a possible underlying mechanism by establishing that the connectome of disorder vulnerability across brain disorders also organizes in accordance with connectional hierarchical gradients like other neurobiological networks. Overall, our results indicate that pairs of within-network regions share a higher relevance for similar cognitive functions and disorders, whereas between-network regions are increasingly implicated in different functions and disorders along the axis of connectional hierarchy.

We also found that the degree of connectional hierarchy, characterized by inter-edge heterogeneity of individual variability, declines with development throughout childhood, adolescence, and adulthood, suggesting that the individual variability becomes more uniform across the connectome edges with development. As previous studies demonstrated that the cortical functional hierarchy evolved in youth[66,67], our results add to the understanding of functional hierarchy development at the connectional level. In line with our finding, a previous study reported that anatomical and functional hierarchies in the cerebellum decline during youth using a similar approach (i.e., heterogeneity)[56].

Several methodological considerations are concerned with interpreting our findings. First, we used a relatively small sample (n < 1,000)[68] to estimate inter-individual variability and connectional hierarchy. To ensure the robustness of our results, we used two independent and well-known high-quality datasets, HCP-D[34] and unrelated HCP-YA[35], which cover different age ranges. Our results showed high similarity in the pattern of individual variability and connectional hierarchy between the two datasets, validating the reliability and reproducibility of our results. Second, the various data modalities of data in our study were acquired from different populations, which potentially magnifies the variance in the connectional hierarchy between these modalities.

However, even when distinct populations are used to define multiscale connectomes, the resulting connectional hierarchy still showed a high correlation, indicating the generalizability of this hierarchical axis to diverse fundamental properties. Finally, our analyses focused on the connections between cortical regions. Future studies should further evaluate connectional hierarchy in subcortical and cerebellar structures.

Notwithstanding these considerations, we identified a novel connectional hierarchy of individual variability across the connectome edges, progressing along a continuous gradient from within-network connections to the edge between sensorimotor and association networks. This hierarchy aligned with a variety of edge-level structural, functional, molecular, cognitive and cross-disorder connectomes, which were shown to progress gradually along a unified axis. Overall, our data revealed a convergent hierarchal organizational principle at the connectional level, bridging multiscale fundamental properties of the human connectome. Our results also revealed that the connectional hierarchy of individual variability was refined during development in youth, providing a novel insight into understanding the neurodevelopmental substrate of the diverse psychiatric disorders, which have been increasingly conceptualized as disorders of brain development[69].

Methods

HCP young adult (HCP-YA) dataset

The present study utilized multi-modal neuroimaging data from 339 unrelated participants (156 males, aged 22-37) in the HCP young adult (HCP-YA) dataset (release S900)[35], including T1-weighted structural MRI, resting-state functional MRI (fMRI), and diffusion MRI. All imaging data were acquired using a multiband sequence on a Siemens 3T Skyra scanner. Structural MRI

data were scanned with a resolution of 0.7mm isotropic. Two resting-state fMRI sessions, with two runs in each session (left-right and right-left phase-encoding), were acquired for each participant with a resolution of 3mm isotropic. Each resting-state run included 1,200 frames and was approximately 15min in length. Diffusion MRI data were acquired in two runs with opposite phase-encoding directions for each participant. Each run included 270 non-collinear directions with 3 non-zero shells (b = 1000, 2000, 3000 s/mm^2). Further details regarding the HCP-YA dataset and MRI acquisition parameters have been described in prior study[35].

HCP development dataset (HCP-D)

In addition to HCP-YA, this study included 633 participants (294 males, aged 8-21) obtained from the HCP-Development (HCP-D) dataset (Release 2.0)[34]. All data were collected using a multiband EPI sequence on a 3T Siemens Prisma scanner. The resolution for structural MRI data was 0.8 mm isotropic. Two resting-state fMRI sessions were acquired for each participant, with two runs in each session, using anterior-posterior (AP) and posterior-anterior (PA) phase-encoding, respectively. Each resting-state run was approximately 6.5min with 488 frames. Considering the shorter scanning length in HCP-D compared to HCP-YA, we added three task-fMRI runs from HCP-D to our analysis. The selected tasks were reward ("guessing"), inhibitory control ("CARIT"), and emotion tasks. Both guessing and CARIT contain two 5min runs, while the emotion task contains one run of 2.5min. All task-fMRI runs were collected with a resolution of 2mm isotropic. Diffusion MRI data included two sessions, each with two shells (b = 1500, 3000 s/mm^2) and 185 diffusion-weighted directions. Further details about the HCP-D dataset have been described in a previous study[70].

The WU-Minn HCP Consortium obtained full informed consent from all participants, and research procedures and ethical guidelines were followed in accordance with the Washington University Institutional Review Boards.

Structural and functional MRI data processing

Minimally preprocessed T1-weighted structural and functional MRI data were acquired from HCP-D and HCP-YA datasets[71]. Structural data were corrected for intensity non-uniformity, skull-stripped, and then used for reconstruction of the cortical surface. Volume-based structural images were segmented into cerebrospinal fluid (CSF), white matter, and gray matter, then spatially normalized to the standard MNI space. Functional MRI data were preprocessed with slice-timing correction, motion correction, distortion correction, co-registration to structural data, normalization to MNI space, and projection to cortical surface. Functional timeseries were resampled to FreeSurfer's fsaverage space, and grayordinates files containing 91k samples were generated.

Pre-processed fMRI data were then post-processed using the eXtensible Connectivity Pipelines (XCP-D)[72]. Volumes with framewise-displacement (FD) greater than 0.3 were flagged as outliers and excluded [73-75]. A total of 36 nuisance regressors were regressed out from the BOLD data, including six motion parameters, global signal, mean white matter signal, and mean CSF signal, along with their temporal derivatives, quadratic terms, and quadratic derivatives[76]. Residual timeseries were then band-pass filtered (0.01-0.08 Hz) and spatially smoothed with a kernel size of FWHM = 6 mm. For the HCP-D dataset, task-evoked activations from selected task-fMRI runs were regressed out by XCP-D, resulting in "pseudo-resting state" timeseries[77] which were then concatenated with the real resting-state functional timeseries for further analysis.

To minimize the potential effects of head motion, we further excluded subjects using two criteria[78]. First, an fMRI run was ruled out if more than 25% of the frames have FD > 0.2 mm. Second, for each fMRI run, we calculated the mean FD distribution by pooling frames from all participants and derived the third quartile (Q3) and interquartile range (IQR) of this distribution. Runs with mean FD greater than 'Q3+1.5×IQR' were excluded. We only included participants whose fMRI runs all fit the above criteria in both HCP-D (4 resting-state and 5 "pseudo-resting state" fMRI runs) and HCP-YA (4 resting-state fMRI runs) datasets. A total of 218 participants from HCP-D and 91 participants from HCP-YA were excluded based on the two criteria. In addition, 3 participants from HCP-YA were further excluded due to incomplete resting-state fMRI runs (less than 1,200 frames). Consequently, 415 participants (179 males, aged 8-21) from HCP-D and 245 participants (114 males, aged 22-35) from HCP-YA datasets were kept for the subsequent analyses.

Diffusion MRI data processing

Diffusion MRI data from HCP-D were preprocessed using QSIPrep (https://qsiprep.readthedocs.io/), an integrative platform for preprocessing and reconstruction of diffusion MRI data[79], which included tools from MRtrix3 (https://www.mrtrix.org/)[80]. Prior to pre-processing, we concatenated the two AP runs and the two PA runs, respectively, and extracted the frames where b-value < 100 s/mm^2 as the b0 image. Next, we applied MP-PCA denoising, Gibbs unringing, and B1 field inhomogeneity correction through MRtrix3's *dwidenoise*[81], *mrdegibbs*[82], and *dwibiascorrect*[83] functions. FSL's eddy was then used for head motion correction and Eddy current correction[84]. Finally, the preprocessed DWI timeseries was resampled to ACPC space at a resolution of 1.5mm isotropic.

We used minimally preprocessed diffusion MRI data from the HCP-YA dataset. The minimal preprocessing pipeline included b0 image intensity normalization across runs, EPI distortion correction, eddy current and motion correction, gradient nonlinearity correction, and registration to the native structural space (1.25 mm). The processed diffusion MRI data were further corrected for B1 field inhomogeneity using MRtrix3.

Functional connectivity measured by BOLD fMRI

We estimated the functional connectivity with fMRI data from both HCP-YA and HCP-D datasets. First, regional BOLD timeseries were extracted using a priori Schaefer parcellation with 400 parcels[36]. Functional connectivity (FC) was calculated as the Pearson correlation coefficient between each pair of regional timeseries, resulting in a 400×400 symmetrical FC matrix for each participant. A Fisher z-transformation was then applied to each FC value in the matrix. Subsequently, the parcels were mapped onto the seven canonical large-scale functional networks from Yeo atlas[37]. We excluded the limbic network in the following analyses as previous studies consistently reported a substantial signal loss in this network[19,38], especially in the orbitofrontal and ventral temporal cortex. As a result, our analysis contains 374 parcels from six functional networks, including visual (VS), somatomotor (SM), dorsal attention (DA), ventral attention (VA), frontoparietal (FP), and default mode (DM). Finally, a 374×374 symmetrical functional connectivity matrix was obtained for each participant. The Schafer atlas with 374 cortical regions were also utilized to construct connectomes from other modalities of data.

Inter-individual variability of functional connectivity and the connectional hierarchy

We estimated the inter-individual variability in functional connectivity and evaluated its organizing principle at the connectional level. Due to the limited number of scans per participant,

a split-session approach[85] was adopted to estimate intra-individual variability. For the HCP-YA dataset, we split each of the four resting-state fMRI runs into three sessions with equal-length timeseries, producing 12 sessions per participant, and acquired 12 functional connectivity matrices for each subject. For the HCP-D dataset, we concatenated 4 resting-state and 5 'pseudo-resting' fMRI runs and split it into 8 sessions. We then acquired eight functional connectivity matrices for each participant in the HCP-D dataset. Inter-individual variability and intra-individual variability of each FC edge (69,751 unique edges in total) were calculated using a linear mixed-effects (LME) model for both HCP-YA and HCP-D datasets[39]. The LME model was implemented with a R package Rex (https://github.com/TingsterX/Reliability_Explorer). This model captures both fixed and random effects, assuming that both the observed response variable and the residual term follow a normal distribution with zero mean and a specific variance. This approach has been used to measure inter-individual and intra-individual variability in previous studies[15,86]. Specifically, for each FC edge, the LME model can be written as follows:

$$FC_{it} = \mu_0 + \lambda_i + \alpha_t + \epsilon_{it}, \text{ where } \lambda_i \sim N(0, \sigma_\lambda^2), \epsilon_t \sim N(0, \sigma_\epsilon^2). \quad (1)$$

Here, i identifies the subject, t indicates the session, λ_i and α_t measures random effect and fixed effect, respectively, and ϵ_{it} is the residual term. The observed individual variation σ_{FC}^2 between FC_{it} can be decomposed into real inter-individual variation σ_b^2 across participants and the intra-individual variations σ_w^2 across sessions (captured by the residual variation σ_ϵ^2). σ_b^2 and σ_w^2 represent inter- and intra-individual variabilities for one specific FC edge, which were used in our following analyses.

For each of our two datasets, we obtained two 374×374 variability matrices for inter-individual and intra-individual variability, respectively. We then scaled the inter-individual variability matrix by dividing the corresponding intra-individual variability with $(\frac{\sigma_b^2}{\sigma_w^2})$ to correct

for intra-individual variations. Furthermore, one may imagine that a larger inter-individual variability could lead to a larger functional connectivity strength; therefore, we controlled for this confounder by scaling with intra-individual variability since the connectivity strength has a similar impact on both variabilities. In this way, we acquired a matrix of inter-individual variability for both HCP-D and HCP-YA datasets. We next compared the similarity in connectional hierarchy between inter-individual variability matrices from the HCP-D dataset and HCP-YA datasets using a Spearman's rank correlation.

We observed a hierarchical gradient in the individual variability matrix along which variability changes continuously from within-network to between-network connections. We termed this edge-level organizing pattern the "connectional hierarchy". For a more straightforward illustration of this connectional hierarchy, we averaged FC variability within each network and between all network pairs, which yielded a 6×6 symmetrical inter-subject FC variability matrix at the network level. The connectional hierarchy of this matrix can be uniquely represented by six within-network FC variability values (the diagonal elements) and fifteen between-network FC variability values (the non-diagonal elements), and these twenty-one unique FC variability values are defined as the connectional hierarchy profile. Then, we calculated the Spearman's rank correlation between connectional hierarchy profiles from HCP-D and HCP-YA datasets. To demonstrate the progression of connectional hierarchy, we sorted within-network and between-network FC variability values in descending order for each functional network. Finally, we grouped the 69,751 unique edges by connection type (i.e., within-sensorimotor, within-association, and between sensorimotor-association) and compared their differences in FC variability using a permutation test (10,000 iterations).

Electromagnetic network at multiple frequency bands with MEG

Resting-state magnetoencephalography (MEG) data for 36 unrelated subjects (20 males, aged 22-35) were obtained from the HCP-YA S900 release and processed with Brainstorm[87] following procedures from a prior study[40]. Notch filtering of 60, 120, 180, 240 and 300 Hz was applied, followed by a high-pass filtering of 0.3 Hz to remove slow-wave and direct current (DC) offset artifacts. For each participant, a source estimation on HCP's fsLR4k cortex surface was obtained using preprocessed sensor-level data, and head models were computed with overlapping spheres. The data covariance matrix was estimated from the resting-state MEG recordings, and regularized by the median eigenvalue method. Then, we obtained each participant's source activity using the linearly constrained minimum variance (LCMV) beamformers method, and parcellated the source-level timeseries using the Schaefer atlas. Finally, MEG connectivity was calculated using amplitude envelope correlation[88] at six electrophysiological frequency bands, delta (2 to 4 Hz), theta (5 to 7 Hz), alpha (8 to 12 Hz), beta (13 to 29 Hz), low-gamma (30 to 59 Hz) and high-gamma (60 to 90 Hz). For each frequency band, the MEG connectivity matrices were averaged across all 36 subjects, and limbic-related edges were removed. To evaluate the electromagnetic basis of connectional hierarchy, we extracted the 69,751 unique edges from the MEG connectivity matrix, and calculated the Spearman's rank correlation between the pattern of individual variability matrix and MEG functional connectivity across all edges for each frequency band.

White matter structural network construction with diffusion MRI

Based on preprocessed diffusion MRI data, a network of structural connectivity (SC) was generated for each participant using reconstructed whole-brain whiter matter tracts. Reconstruction was completed using the *mrtrix_multishell_msmt_ACT-hsvs* method in MRtrix3, which implemented a multi-shell, multi-tissue constrained spherical deconvolution (CSD) to estimate the fiber orientation distribution (FOD) for each voxel[43]. We used the anatomically constrained

tractography (ACT) framework to improve the biological accuracy of fiber reconstruction[44]. Specifically, the tractography was performed by *tckgen*, which generates 40 million streamlines (length range from 30mm to 250mm, FOD power = 0.33) using an improved probabilistic streamlines tractography (iFOD2) based on the second-order integration over FOD. We selectively filtered the streamlines from the tractogram based on the spherical deconvolution of the diffusion signal and estimated the streamline weights using the command *tcksift2*[45]. Next, the structural connectivity matrix was constructed using *tck2connectome* with the Schaefer-400 atlas as an a priori cortical atlas. The weight of each structural connectivity indicates the number of streamlines connecting two regions. The edge weights were normalized by dividing the average volume of the two regions[89], and then log-transformed. Edges with a weight of 0 in any participant were set to 0 for all participants[90]. Then, we averaged the SC matrix across all participants in each dataset, and removed limbic-related regions and edges, resulting in a 374×374 SC matrix. To evaluate the structural connectivity basis of the connectional hierarchy, we calculated the Spearman's rank correlation of connection strength between SC network and individual variability network across all edges with non-zero streamline counts.

Correlated gene expression network

We obtained gene expression data from the Allen Human Brain Atlas (AHBA, https://human.brain-map.org)[49], a public transcriptional atlas containing DNA microarrays sampled from six postmortem human brains (5 males, aged 24-57). Microarray data were available in the left hemisphere for four of the donors, and two donors contributed tissue samples from both hemispheres. Using the Schaefer-400 atlas in MNI space, we processed regional microarray expression data with the abagen toolbox (version 0.1.3; https://github.com/rmarkello/abagen)[91].

In this study, we followed the protocol outlined by the toolbox to obtain the desired information, noted in italic as follows. *First, microarray probes were reannotated using data provided by Arnatkevičiūtė et al.[92]; probes that did not match a valid Entrez ID were discarded. Next, probes were filtered based on their expression intensity relative to background noise[93], such that probes with intensity less than the background in ≥ 50.00% of samples across donors were discarded, yielding 31,569 probes. When multiple probes indexed the expression of the same gene, we selected and used the probe with the most consistent pattern of regional variation across donors (i.e., differential stability[94]), calculated with:*

$$\Delta_S(p) = \frac{1}{\binom{N}{2}} \sum_{i=1}^{N-1} \sum_{j=i+1}^{N} \rho\left[B_i(p), B_j(p)\right] \quad (2)$$

where ρ is Spearman's rank correlation of the expression of a single probe, p, across regions in two donors B_i and B_j, and N is the total number of donors. Here, regions correspond to the structural designations provided in the ontology from the AHBA.

The MNI coordinates of tissue samples were updated to those generated via non-linear registration using the Advanced Normalization Tools (ANTs; https://github.com/ANTsX/ANTs). To increase spatial coverage, tissue samples were mirrored bilaterally across the left and right hemispheres[95]. Samples were assigned to brain regions in the provided atlas if their MNI coordinates were within 2 mm of a given parcel. If a brain region was not assigned a tissue sample based on the above procedure, every voxel in the region was mapped to the nearest tissue sample from the donor in order to generate a dense, interpolated expression map. The average of these expression values was taken across all voxels in the region, weighted by the distance between each voxel and the sample mapped to it, in order to obtain an estimate of the parcellated expression

values for the missing region. All tissue samples not assigned to a brain region in the provided atlas were discarded.

Inter-subject variation was addressed by normalizing tissue sample expression values across genes using a robust sigmoid function[96]*:*

$$x_{norm} = \frac{1}{1 + exp\left(-\frac{(x_g - \langle x_g \rangle)}{IQR_x}\right)} \quad (3)$$

where ⟨x⟩ is the median and IQR_x is the normalized interquartile range of the expression of a single tissue sample across genes. Normalized expression values were then rescaled to the unit interval:

$$x_{scaled} = \frac{x_{norm} - min(x_{norm})}{max(x_{norm}) - min(x_{norm})} \quad (4)$$

Gene expression values were then normalized across tissue samples using an identical procedure. Samples assigned to the same brain region were averaged separately for each donor and then across donors, yielding a regional expression matrix for each donor with 400 rows, corresponding to brain regions, and 15,633 columns, corresponding to the retained genes. Additionally, we constrained our analysis to 2,256 brain-specific genes according to previous studies[16,97].

We then constructed a correlated gene expression network (374×374, without limbic network) by computing pairwise Pearson correlation between regional transcriptional profiles (1×2,256). Here, higher inter-regional transcriptional similarity indicates modulation by similar genes. We excluded limbic network related nodes and edges, and flattened the lower triangle of the correlated gene expression network into a vector. Spearman's rank correlation was performed between the two vectors derived from the correlated gene expression matrix and individual variability matrix of functional connectivity to quantify the underlying genetic basis of connectional hierarchy.

Similarity network of neurotransmitter receptor expression

The similarity network of neurotransmitter receptor expression was constructed using profiles of regional expression provided by previous studies[27]. The dataset used in this study contains PET images of the density of 19 different receptors and transporters acquired from 1,238 healthy participants (718 males). These receptors and transporters function in diverse neurotransmitter systems, including dopamine, norepinephrine, serotonin, acetylcholine, glutamate, GABA, histamine, cannabinoid and opioid systems. Receptors and transporters with more than one image of the same tracer were averaged. For each type of PET map, all images were registered to the ICBM-152 template (2009c version), and regional receptor density was mapped onto the Schaefer-400 atlas, resulting in 400 regional average values. Regional density values were z-scored and combined across receptor types, resulting in a region×receptor matrix (400×19). We acquired this matrix from shared resources from Hansen and colleagues[27], which is available at (https://github.com/netneurolab/hansen_receptors). We next computed the Pearson correlation of the density between each two brain regions across the 19 types of receptors and transporters, resulting in a 374×374 network of between-regional similarity in receptor density after excluding the limbic network, termed the "receptor similarity network". We calculated the Spearman's rank correlation between the receptor similarity matrix and functional connectivity variability matrix to characterize the neurotransmitter basis of connectional hierarchy. More details regarding the PET dataset can be found in the aforementioned study[27].

Similarity network of cognitive relevance

We selected 123 terms related to neurocognitive processes[22] using the Cognitive Atlas[51], an ontology database of cognitive science and neuroscience, for constructing the similarity network

of cognitive relevance. These terms ranged from umbrella terms (e.g., "attention") to specific cognitive processes (e.g., "episodic memory"), emotional states (e.g., "fear" and "anxiety") and behaviors (e.g., "sleep"). We generated an activation probability map for each term using Neurosynth (https://github.com/neurosynth/neurosynth)[50], a meta-analytical toolbox referencing cognitive terms to brain voxel positions by searching over 15,000 fMRI studies. For each term of interest (e.g., "emotion"), the coordinates of activated voxels were collected and a whole-brain activation probability map was generated.

We projected average regional activation probabilities onto the a priori Schaefer atlas, resulting in a region×cognition matrix (374×123) where values represent the activation probability of each region for a selected cognitive term. We next generated the network of cognitive relevance by computing the Pearson correlation of regional activation probability between each pair of brain regions across the 123 cognitive terms. A higher correlation indicates that two brain regions are more likely to be activated in similar cognitive processes. We next calculated the Spearman's rank correlation between individual variability in functional connectivity and the cognitive similarity network, to evaluate the implications of connectional hierarchy in cognition.

Similarity network of disorder vulnerability

We estimated the similarity network of disorder vulnerability by computing the correlation of regional cortical abnormalities between any two brain regions across multiple brain disorders[52]. We obtained statistical maps of cortical thickness abnormalities for 13 neurological, neurodevelopmental and psychiatric disorders from the Enhancing Neuroimaging Genetics through Meta-Analysis (ENIGMA) consortium[53] and the ENIGMA toolbox (https://github.com/MICA-MNI/ENIGMA)[54]. Specifically, cortical thickness abnormality maps for 10 brain disorders were acquired from the ENIGMA toolbox, including 22q11.2 deletion

syndrome (patients, $n = 474$; controls, $n = 315$)[98], attention-deficit/hyperactivity disorder (patients, $n = 733$; controls, $n = 539$)[99], autism spectrum disorder (patients, $n = 1,571$; controls, $n = 1,651$)[100], epilepsy (idiopathic generalized, $n = 367$; right temporal lobe, $n = 339$; left temporal lobe, $n = 415$; and 1,727 controls)[101], depression (patients, $n = 2,148$; controls, $n = 7,957$)[102], obsessive-compulsive disorder (patients, $n = 1,905$; controls, $n = 1,760$)[103], schizophrenia (patients, $n = 4,474$; controls, $n = 5,098$)[104], and bipolar disorder (patients, $n = 1,837$; controls, $n = 2,582$)[105]. Maps for the other three disorders were acquired from supplementary materials of prior studies, including obesity (patients, n = 1,223; controls, n = 2,917)[106], schizotypy (n = 3,004)[107], and Parkinson's disease (patients, n = 2,367; controls, n = 1,183)[108].

The maps of cortical thickness abnormalities were acquired by standardized pipelines in prior literature (http://enigma.ini.usc.edu/protocols/; see the above paragraph for a series of related studies). Specifically, regional average cortical thickness was calculated based on the Desikan–Killiany atlas with 68 cortical regions (DK-68)[55]. Then, the case-control differences in regional cortical thickness were statistically compared for each brain disorder and the effect sizes (Cohen's d) were computed based on statistical t-values. As there was only one group for schizotypy, the effects size (r) was measured by the Pearson correlation between schizotypy scores and regional cortical thickness. Except for autism spectrum disorder, ENIGMA toolbox provided the statistical effect size values for several different age ranges and we utilized the data for adults in this study. For autism, only one statistical map was provided across all participants (aged 2-64).

Based on the above analyses, we examined 68 regional statistical effect sizes for each of the 13 brain disorders. We next generated the disorders similarity network (68×68) by computing Pearson correlation between the abnormality profiles (1×13) of any two cortical regions. We re-estimated the individual variability of functional connectivity using the 68 cortical regions for

HCP-D and HCP-YA datasets, respectively. We then compared the disorder similarity network and individual variability network across all edges using Spearman's rank correlation, to evaluate the implications of connectional hierarchy in brain disorders. Considering the inaccurate assignment from the DK-68 atlas to Yeo's 7 networks, we did not analyze the network-averaged results here.

Null models for between-network correlations

To evaluate the statistical significance of the correlation between the two networks, we generated null models for networks similarly as did in spatial permutation testing for the comparison of cortical properties[109]. Specifically, we generated the null networks by randomly rearranging the order of brain regions (nodes) in the matrix. Taking the matrix estimated by 374 cortical regions from the Schaefer atlas as an example, the original order of node IDs in both columns and rows of the matrix is from 1 to 374. We shuffled the order of node IDs of both the columns and rows, so that the same node ID could represent different brain regions across different randomized networks. This null network preserves the mean and variance of the matrix, it also ensures that the regional profile (the column of the matrix, 374×1) includes all the 374 cortical regions. With this approach, we constructed the null distribution by generating 50,000 randomized individual variability networks and calculated their Spearman's rank correlation with other networks, including hemodynamic and electromagnetic functional connectivity, structural network, correlated gene expression network, correlated neurotransmitter receptor expression network, the network of cognitive relevance and the network of disorder vulnerability. We compared the correlation value obtained by the empirical individual variability network with the ones acquired with the null networks to determine the significance level, and The P value of this permutation testing (P_{perm}) was reported. As we have compared the connectional hierarchy of individual

variability with multiple connectomes derived from other modalities in two datasets, we performed a Bonferroni correction to correct for multiple comparisons.

Development of connectional hierarchy in youth

To explore the maturation of connectional hierarchy in youth, we re-grouped the HCP-D participants (8~21 years old) into 14 age groups with a one-year gap, and calculated the inter-individual variability matrix for each group. As done in a previous study[56], we evaluated connectional hierarchy with the inter-edge heterogeneity of individual variability of between-network edges, to summarize the degree of connectional hierarchy. Specifically, we extracted 6 within-network and 15 between-network variability values from the network-level inter-individual variability matrix (6×6). The degree of connection hierarchy was defined as the inter-edge heterogeneity of individual variability, which we quantified as the median absolute deviation across these 21 variability values. With this approach, we estimated inter-edge heterogeneity of individual variability for each of the 14 age groups and evaluated the developmental changes in connectional hierarchy from 8 to 21 years old. To model both linear and nonlinear developmental effects, we used a generalized additive model (GAM)[60] with penalized splines, which estimates nonlinearities using restricted maximum likelihood (REML) and penalizes nonlinearity in order to avoid over-fitting the data. The mean age across participants was calculated for each age group and used in the GAM. The mean age was modeled using a penalized spline, while including sex and in-scanner head motion as model covariates, as follows:

$$Inter\text{-}edge\ heterogeneity \sim s(Age,\ k = 4) + Sex + Motion \quad (5)$$

where $s()$ is the spline basis function, and k is the basis dimension for smooths. As the analyses were performed at the group level, the sex in the GAM is represented by the male/female ratio of participants for a particular age group, and the motion was calculated by averaging the mean FD

across all individuals and all runs within each age group. To demonstrate the association between inter-edge heterogeneity and age more intuitively, the p value of $s(Age)$ was transformed to a Z value, and a partial correlation was also performed with sex and motion controlled.

Validation analysis for controlling inter-regional distance

Prior studies reported that adjacent brain regions are modulated by analogous underlying molecular and structural basis and exhibit similar functions[27,61,63]. To account for the effects of inter-regional distance, we calculated the Euclidean distance between every two cortical regions in the MNI space for the Schaefer-400 atlas and DK-68 atlas, respectively. We regressed out the inter-regional distance from the inter-individual variability matrix as well as all other networks and re-estimated their correlations according to the previous analysis. Similarly, we controlled the effects of inter-regional distance in the development analysis by regressing out the inter-regional distance from the inter-individual variability matrix of each age group, and re-estimated the association between age and connectional hierarchy.

Data availability

Connectional hierarchy measured by individual variability in functional connectivity, and additional connectivity matrices (hemodynamic connectivity, MEG connectivity, structural connectivity, transcriptional similarity, receptor similarity, cognitive similarity and disorder similarity) can be found at https://github.com/CuiLabCIBR/Connectional_Hierarchy. In particular, the HCP-YA and HCP-D datasets, including T1-weight MRI, functional MRI, diffusion-weighted MRI, and MEG are available at https://db.humanconnectome.org/. Gene expression data can be downloaded from the AHBA (http://human.brain-map.org) and processed using the abagen toolbox (https://github.com/rmarkello/abagen). The 19 PET maps for neurotransmitter receptors

and transporters profiles can be obtained from the neuromaps toolbox (https://github.com/netneurolab/neuromaps; ref.[29]), and the region×receptor matrix is available at (https://github.com/netneurolab/hansen_receptors; ref.[27]). The 123 cognitive terms were selected from the Cognitive Atlas (https://www.cognitiveatlas.org/), and corresponding cognitive activation probability maps were obtained from the Neurosynth using the neurosynth toolbox (https://github.com/neurosynth/neurosynth). Cortical thickness abnormality maps for 13 disorders are available through the ENIGMA consortium using the ENIGMA toolbox (https://github.com/MICA-MNI/ENIGMA).

Code availability

All code used to perform the analyses in this study can be found at https://github.com/CuiLabCIBR/Connectional_Hierarchy.

ACKNOWLEDGEMENTS

This work is supported by the STI 2030-Major Projects (2022ZD0211300), Beijing Nova Program (Z211100002121002), and CIBR funds. Data were provided [in part] by the Human Connectome Project, WU-Minn Consortium (Principal Investigators: David Van Essen and Kamil Ugurbil; 1U54MH091657) funded by the 16 NIH Institutes and Centers that support the NIH Blueprint for Neuroscience Research; and by the McDonnell Center for Systems Neuroscience at Washington University. The HCP-Development 2.0 Release data used in this report came from DOI: 10.15154/1520708. Research reported in this publication was supported by the National Institute of Mental Health of the National Institutes of Health under Award Number U01MH109589 and by funds provided by the McDonnell Center for Systems Neuroscience at Washington University in St. Louis.

AUTHOR CONTRIBUTIONS

Z.C., H.Y, and G.W. designed the study. H.Y. and G.W. performed the analyses with support from Y.L. and Y.M. H.Y. created the figures. Z.C. supervised the project. R.C., A.P., T.X., V.S., T.S. commented on analyses. H.Y., G.W., and Z.C. wrote the manuscript with review and editing from all other authors.

References

1 Finn, E. S. *et al.* Functional connectome fingerprinting: identifying individuals using patterns of brain connectivity. *Nat Neurosci* **18**, 1664-1671, doi:10.1038/nn.4135 (2015).

2 Mueller, S. *et al.* Individual variability in functional connectivity architecture of the human brain. *Neuron* **77**, 586-595, doi:10.1016/j.neuron.2012.12.028 (2013).

3 Cui, Z. *et al.* Individual Variation in Functional Topography of Association Networks in Youth. *Neuron* **106**, 340-353, doi:10.1016/j.neuron.2020.01.029 (2020).

4 Sydnor, V. J. *et al.* Neurodevelopment of the association cortices: Patterns, mechanisms, and implications for psychopathology. *Neuron* (2021).

5 Li, M. *et al.* Performing group-level functional image analyses based on homologous functional regions mapped in individuals. *PLoS Biol* **17**, e2007032, doi:10.1371/journal.pbio.2007032 (2019).

6 Hilgetag, C. C. & Goulas, A. 'Hierarchy' in the organization of brain networks. *Philos Trans R Soc Lond B Biol Sci* **375**, 20190319, doi:10.1098/rstb.2019.0319 (2020).

7 Sporns, O., Tononi, G. & Kotter, R. The human connectome: A structural description of the human brain. *PLoS Comput Biol* **1**, e42, doi:10.1371/journal.pcbi.0010042 (2005).

8 Bullmore, E. & Sporns, O. Complex brain networks: graph theoretical analysis of structural and functional systems. *Nature reviews. Neuroscience* **10**, 186-198, doi:10.1038/nrn2575 (2009).

9 Smith, S. M. *et al.* A positive-negative mode of population covariation links brain connectivity, demographics and behavior. *Nat Neurosci* **18**, 1565-1567, doi:10.1038/nn.4125 (2015).

10 van den Heuvel, M. P. & Sporns, O. A cross-disorder connectome landscape of brain dysconnectivity. *Nature reviews. Neuroscience*, doi:10.1038/s41583-019-0177-6 (2019).

11 Zhang, Y. *et al.* Identification of psychiatric disorder subtypes from functional connectivity patterns in resting-state electroencephalography. *Nat Biomed Eng* **5**, 309-323, doi:10.1038/s41551-020-00614-8 (2021).

12 Sydnor, V. J. *et al.* Cortical-subcortical structural connections support transcranial magnetic stimulation engagement of the amygdala. *bioRxiv* (2021).

13 Scangos, K. W. *et al.* Closed-loop neuromodulation in an individual with treatment-resistant depression. *Nature medicine* **27**, 1696-1700, doi:10.1038/s41591-021-01480-w (2021).

14 Laumann, T. O. *et al.* Functional System and Areal Organization of a Highly Sampled Individual Human Brain. *Neuron* **87**, 657-670, doi:10.1016/j.neuron.2015.06.037 (2015).

15 O'Connor, D. *et al.* The Healthy Brain Network Serial Scanning Initiative: a resource for evaluating inter-individual differences and their reliabilities across scan conditions and sessions. *Gigascience* **6**, 1-14, doi:10.1093/gigascience/giw011 (2017).

16 Burt, J. B. *et al.* Hierarchy of transcriptomic specialization across human cortex captured by structural neuroimaging topography. *Nat Neurosci* **21**, 1251-1259, doi:10.1038/s41593-018-0195-0 (2018).

17 Mesulam, M. M. From sensation to cognition. *Brain* **121 (Pt 6)**, 1013-1052, doi:10.1093/brain/121.6.1013 (1998).

18 Margulies, D. S. *et al.* Situating the default-mode network along a principal gradient of macroscale cortical organization. *Proc Natl Acad Sci U S A* **113**, 12574-12579, doi:10.1073/pnas.1608282113 (2016).

19 Raut, R. V., Snyder, A. Z. & Raichle, M. E. Hierarchical dynamics as a macroscopic organizing principle of the human brain. *Proc Natl Acad Sci U S A* **117**, 20890-20897, doi:10.1073/pnas.2003383117 (2020).

20 Reardon, P. K. *et al.* Normative brain size variation and brain shape diversity in humans. *Science* **360**, 1222-1227, doi:10.1126/science.aar2578 (2018).

21 Huntenburg, J. M., Bazin, P. L. & Margulies, D. S. Large-Scale Gradients in Human Cortical Organization. *Trends Cogn Sci* **22**, 21-31, doi:10.1016/j.tics.2017.11.002 (2018).

22 Hansen, J. Y. *et al.* Mapping gene transcription and neurocognition across human neocortex. *Nat Hum Behav* **5**, 1240-1250, doi:10.1038/s41562-021-01082-z (2021).

23 Demirtas, M. *et al.* Hierarchical Heterogeneity across Human Cortex Shapes Large-Scale Neural Dynamics. *Neuron* **101**, 1181-1194 e1113, doi:10.1016/j.neuron.2019.01.017 (2019).

24 Wang, X. J. Macroscopic gradients of synaptic excitation and inhibition in the neocortex. *Nature reviews. Neuroscience* **21**, 169-178, doi:10.1038/s41583-020-0262-x (2020).

25 Glasser, M. F. & Van Essen, D. C. Mapping human cortical areas in vivo based on myelin content as revealed by T1- and T2-weighted MRI. *The Journal of neuroscience : the official journal of the Society for Neuroscience* **31**, 11597-11616, doi:10.1523/JNEUROSCI.2180-11.2011 (2011).

26 Hill, J. *et al.* Similar patterns of cortical expansion during human development and evolution. *Proc Natl Acad Sci U S A* **107**, 13135-13140, doi:10.1073/pnas.1001229107 (2010).

27 Hansen, J. Y. *et al.* Mapping neurotransmitter systems to the structural and functional organization of the human neocortex. *Nat Neurosci*, doi:10.1038/s41593-022-01186-3 (2022).

28 Goulas, A. *et al.* The natural axis of transmitter receptor distribution in the human cerebral cortex. *Proc Natl Acad Sci U S A* **118**, doi:10.1073/pnas.2020574118 (2021).

29 Markello, R. D. *et al.* neuromaps: structural and functional interpretation of brain maps. *Nat Methods* **19**, 1472-1479, doi:10.1038/s41592-022-01625-w (2022).

30 Goulas, A., Zilles, K. & Hilgetag, C. C. Cortical Gradients and Laminar Projections in Mammals. *Trends in neurosciences* **41**, 775-788, doi:10.1016/j.tins.2018.06.003 (2018).

31 Paquola, C. *et al.* A multi-scale cortical wiring space links cellular architecture and functional dynamics in the human brain. *PLoS Biol* **18**, e3000979, doi:10.1371/journal.pbio.3000979 (2020).

32 Xu, T. *et al.* Cross-species functional alignment reveals evolutionary hierarchy within the connectome. *Neuroimage* **223**, 117346, doi:10.1016/j.neuroimage.2020.117346 (2020).

33 Pines, A. R. *et al.* Dissociable multi-scale patterns of development in personalized brain networks. *Nat Commun* **13**, 2647, doi:10.1038/s41467-022-30244-4 (2022).

34 Somerville, L. H. *et al.* The Lifespan Human Connectome Project in Development: A large-scale study of brain connectivity development in 5-21 year olds. *Neuroimage* **183**, 456-468, doi:10.1016/j.neuroimage.2018.08.050 (2018).

35 Van Essen, D. C. *et al.* The WU-Minn Human Connectome Project: an overview. *Neuroimage* **80**, 62-79, doi:10.1016/j.neuroimage.2013.05.041 (2013).

36 Schaefer, A. *et al.* Local-Global Parcellation of the Human Cerebral Cortex from Intrinsic Functional Connectivity MRI. *Cereb Cortex* **28**, 3095-3114, doi:10.1093/cercor/bhx179 (2018).

37 Yeo, B. T. *et al.* The organization of the human cerebral cortex estimated by intrinsic functional connectivity. *J Neurophysiol* **106**, 1125-1165, doi:10.1152/jn.00338.2011 (2011).

38 Wig, G. S. *et al.* Parcellating an individual subject's cortical and subcortical brain structures using snowball sampling of resting-state correlations. *Cereb Cortex* **24**, 2036-2054, doi:10.1093/cercor/bht056 (2014).

39 Xu, T. *et al.* A Guide for Quantifying and Optimizing Measurement Reliability for the Study of Individual Differences. *bioRxiv*, 2022.2001. 2027.478100 (2022).

40 Shafiei, G., Baillet, S. & Misic, B. Human electromagnetic and haemodynamic networks systematically converge in unimodal cortex and diverge in transmodal cortex. *PLoS Biol* **20**, e3001735, doi:10.1371/journal.pbio.3001735 (2022).

41 Avena-Koenigsberger, A., Misic, B. & Sporns, O. Communication dynamics in complex brain networks. *Nat Rev Neurosci.* **19**, 17-33, doi:10.1038/nrn.2017.149 (2017).

42 Suarez, L. E., Markello, R. D., Betzel, R. F. & Misic, B. Linking Structure and Function in Macroscale Brain Networks. *Trends Cogn Sci* **24**, 302-315, doi:10.1016/j.tics.2020.01.008 (2020).

43 Jeurissen, B., Tournier, J. D., Dhollander, T., Connelly, A. & Sijbers, J. Multi-tissue constrained spherical deconvolution for improved analysis of multi-shell diffusion MRI data. *Neuroimage* **103**, 411-426, doi:10.1016/j.neuroimage.2014.07.061 (2014).

44 Smith, R. E., Tournier, J.-D., Calamante, F. & Connelly, A. Anatomically-constrained tractography: improved diffusion MRI streamlines tractography through effective use of anatomical information. *Neuroimage* **62**, 1924-1938 (2012).

45 Smith, R. E., Tournier, J. D., Calamante, F. & Connelly, A. SIFT2: Enabling dense quantitative assessment of brain white matter connectivity using streamlines tractography. *Neuroimage* **119**, 338-351, doi:10.1016/j.neuroimage.2015.06.092 (2015).

46 Richiardi, J. *et al.* Correlated gene expression supports synchronous activity in brain networks. *Science* **348**, 1241-1244, doi:10.1126/science.1255905 (2015).

47 Anderson, K. M. *et al.* Gene expression links functional networks across cortex and striatum. *Nat Commun* **9**, 1428, doi:10.1038/s41467-018-03811-x (2018).

48 Krienen, F. M., Yeo, B. T., Ge, T., Buckner, R. L. & Sherwood, C. C. Transcriptional profiles of supragranular-enriched genes associate with corticocortical network architecture in the human brain. *Proc Natl Acad Sci U S A* **113**, E469-478, doi:10.1073/pnas.1510903113 (2016).

49 Hawrylycz, M. J. *et al.* An anatomically comprehensive atlas of the adult human brain transcriptome. *Nature* **489**, 391-399, doi:10.1038/nature11405 (2012).

50 Yarkoni, T., Poldrack, R. A., Nichols, T. E., Van Essen, D. C. & Wager, T. D. Large-scale automated synthesis of human functional neuroimaging data. *Nature methods* **8**, 665-670 (2011).

51 Poldrack, R. A. *et al.* The cognitive atlas: toward a knowledge foundation for cognitive neuroscience. *Front Neuroinform* **5**, 17, doi:10.3389/fninf.2011.00017 (2011).

52 Hansen, J. Y. *et al.* Local molecular and global connectomic contributions to cross-disorder cortical abnormalities. *Nat Commun* **13**, 4682, doi:10.1038/s41467-022-32420-y (2022).

53 Thompson, P. M. *et al.* ENIGMA and global neuroscience: A decade of large-scale studies of the brain in health and disease across more than 40 countries. *Transl Psychiatry* **10**, 100, doi:10.1038/s41398-020-0705-1 (2020).

54 Lariviere, S. *et al.* The ENIGMA Toolbox: multiscale neural contextualization of multisite neuroimaging datasets. *Nat Methods* **18**, 698-700, doi:10.1038/s41592-021-01186-4 (2021).

55 Desikan, R. S. *et al.* An automated labeling system for subdividing the human cerebral cortex on MRI scans into gyral based regions of interest. *Neuroimage* **31**, 968-980, doi:10.1016/j.neuroimage.2006.01.021 (2006).

56 Liu, X., d'Oleire Uquillas, F., Viaene, A. N., Zhen, Z. & Gomez, J. A multifaceted gradient in human cerebellum of structural and functional development. *Nat Neurosci* **25**, 1129-1133, doi:10.1038/s41593-022-01136-z (2022).

57 Cui, Z. *et al.* Optimization of energy state transition trajectory supports the development of executive function during youth. *eLife* **9**, doi:10.7554/eLife.53060 (2020).

58 Satterthwaite, T. D. *et al.* Impact of puberty on the evolution of cerebral perfusion during adolescence. *Proc Natl Acad Sci U S A* **111**, 8643-8648, doi:10.1073/pnas.1400178111 (2014).

59 Bethlehem, R. A. I. *et al.* Brain charts for the human lifespan. *Nature* **604**, 525-533, doi:10.1038/s41586-022-04554-y (2022).

60 Wood, S. N. Stable and efficient multiple smoothing parameter estimation for generalized additive models. *J Am Stat Assoc* **99**, 673-686 (2004).

61 Betzel, R. F. & Bassett, D. S. Specificity and robustness of long-distance connections in weighted, interareal connectomes. *Proc Natl Acad Sci U S A* **115**, E4880-E4889, doi:10.1073/pnas.1720186115 (2018).

62 Betzel, R. F. *et al.* Structural, geometric and genetic factors predict interregional brain connectivity patterns probed by electrocorticography. *Nat Biomed Eng* **3**, 902-916, doi:10.1038/s41551-019-0404-5 (2019).

63 Roberts, J. A. *et al.* The contribution of geometry to the human connectome. *Neuroimage* **124**, 379-393, doi:10.1016/j.neuroimage.2015.09.009 (2016).

64 Collins, C. E., Airey, D. C., Young, N. A., Leitch, D. B. & Kaas, J. H. Neuron densities vary across and within cortical areas in primates. *Proc Natl Acad Sci U S A* **107**, 15927-15932, doi:10.1073/pnas.1010356107 (2010).

65 Hansen, J. Y. *et al.* Multimodal, multiscale connectivity blueprints of the cerebral cortex. *bioRxiv*, 2022.2012. 2002.518906 (2022).

66 Xia, Y. *et al.* Development of functional connectome gradients during childhood and adolescence. *Sci Bull (Beijing)* **67**, 1049-1061, doi:10.1016/j.scib.2022.01.002 (2022).

67 Dong, H. M., Margulies, D. S., Zuo, X. N. & Holmes, A. J. Shifting gradients of macroscale cortical organization mark the transition from childhood to adolescence. *Proc Natl Acad Sci U S A* **118**, doi:10.1073/pnas.2024448118 (2021).

68 Marek, S. *et al.* Reproducible brain-wide association studies require thousands of individuals. *Nature* **603**, 654-660, doi:10.1038/s41586-022-04492-9 (2022).

69 Insel, T. R. Mental disorders in childhood: shifting the focus from behavioral symptoms to neurodevelopmental trajectories. *Jama* **311**, 1727-1728, doi:10.1001/jama.2014.1193 (2014).

70 Harms, M. P. *et al.* Extending the Human Connectome Project across ages: Imaging protocols for the Lifespan Development and Aging projects. *Neuroimage* **183**, 972-984, doi:10.1016/j.neuroimage.2018.09.060 (2018).

71 Glasser, M. F. *et al.* The minimal preprocessing pipelines for the Human Connectome Project. *Neuroimage* **80**, 105-124, doi:10.1016/j.neuroimage.2013.04.127 (2013).

72 Ciric, R. *et al.* Mitigating head motion artifact in functional connectivity MRI. *Nat Protoc* **13**, 2801-2826, doi:10.1038/s41596-018-0065-y (2018).

73 Satterthwaite, T. D. *et al.* An improved framework for confound regression and filtering for control of motion artifact in the preprocessing of resting-state functional connectivity data. *Neuroimage* **64**, 240-256, doi:10.1016/j.neuroimage.2012.08.052 (2013).

74 Power, J. D. *et al.* Methods to detect, characterize, and remove motion artifact in resting state fMRI. *Neuroimage* **84**, 320-341, doi:10.1016/j.neuroimage.2013.08.048 (2014).

75 Satterthwaite, T. D. *et al.* Heterogeneous impact of motion on fundamental patterns of developmental changes in functional connectivity during youth. *Neuroimage* **83**, 45-57, doi:10.1016/j.neuroimage.2013.06.045 (2013).

76 Ciric, R. *et al.* Benchmarking of participant-level confound regression strategies for the control of motion artifact in studies of functional connectivity. *Neuroimage*, doi:10.1016/j.neuroimage.2017.03.020 (2017).

77 Fair, D. A. *et al.* A method for using blocked and event-related fMRI data to study "resting state" functional connectivity. *Neuroimage* **35**, 396-405, doi:10.1016/j.neuroimage.2006.11.051 (2007).

78 Faskowitz, J., Esfahlani, F. Z., Jo, Y., Sporns, O. & Betzel, R. F. Edge-centric functional network representations of human cerebral cortex reveal overlapping system-level architecture. *Nat Neurosci* **23**, 1644-1654, doi:10.1038/s41593-020-00719-y (2020).

79 Cieslak, M. *et al.* QSIPrep: an integrative platform for preprocessing and reconstructing diffusion MRI data. *Nat Methods*, doi:10.1038/s41592-021-01185-5 (2021).

80 Tournier, J. D. *et al.* MRtrix3: A fast, flexible and open software framework for medical image processing and visualisation. *Neuroimage* **202**, 116137, doi:10.1016/j.neuroimage.2019.116137 (2019).

81 Veraart, J. *et al.* Denoising of diffusion MRI using random matrix theory. *Neuroimage* **142**, 394-406, doi:10.1016/j.neuroimage.2016.08.016 (2016).

82 Kellner, E., Dhital, B., Kiselev, V. G. & Reisert, M. Gibbs-ringing artifact removal based on local subvoxel-shifts. *Magnetic resonance in medicine : official journal of the Society of Magnetic Resonance in Medicine / Society of Magnetic Resonance in Medicine* **76**, 1574-1581, doi:10.1002/mrm.26054 (2016).

83 Tustison, N. J. *et al.* N4ITK: improved N3 bias correction. *IEEE transactions on medical imaging* **29**, 1310-1320, doi:10.1109/TMI.2010.2046908 (2010).

84 Andersson, J. L. R., Graham, M. S., Zsoldos, E. & Sotiropoulos, S. N. Incorporating outlier detection and replacement into a non-parametric framework for movement and distortion correction of diffusion MR images. *Neuroimage* **141**, 556-572, doi:10.1016/j.neuroimage.2016.06.058 (2016).

85 Mueller, S. *et al.* Reliability correction for functional connectivity: Theory and implementation. *Hum Brain Mapp* **36**, 4664-4680, doi:10.1002/hbm.22947 (2015).

86 Yang, Z. *et al.* Measurement reliability for individual differences in multilayer network dynamics: Cautions and considerations. *Neuroimage* **225**, 117489, doi:10.1016/j.neuroimage.2020.117489 (2021).

87 Tadel, F., Baillet, S., Mosher, J. C., Pantazis, D. & Leahy, R. M. Brainstorm: a user-friendly application for MEG/EEG analysis. *Comput Intell Neurosci* **2011**, 879716, doi:10.1155/2011/879716 (2011).

88 Bruns, A., Eckhorn, R., Jokeit, H. & Ebner, A. Amplitude envelope correlation detects coupling among incoherent brain signals. *Neuroreport* **11**, 1509-1514 (2000).

89 Hagmann, P. *et al.* Mapping the structural core of human cerebral cortex. *PLoS Biol* **6**, e159, doi:10.1371/journal.pbio.0060159 (2008).

90 Zhao, C. *et al.* Hemispheric Module-Specific Influence of the X Chromosome on White Matter Connectivity: Evidence from Girls with Turner Syndrome. *Cereb Cortex* **29**, 4580-4594, doi:10.1093/cercor/bhy335 (2019).

91 Markello, R. D. *et al.* Standardizing workflows in imaging transcriptomics with the abagen toolbox. *Elife* **10**, doi:10.7554/eLife.72129 (2021).

92 Arnatkeviciute, A., Fulcher, B. D. & Fornito, A. A practical guide to linking brain-wide gene expression and neuroimaging data. *Neuroimage* **189**, 353-367, doi:10.1016/j.neuroimage.2019.01.011 (2019).

93 Quackenbush, J. Microarray data normalization and transformation. *Nat Genet* **32 Suppl**, 496-501, doi:10.1038/ng1032 (2002).

94 Hawrylycz, M. *et al.* Canonical genetic signatures of the adult human brain. *Nat Neurosci* **18**, 1832-1844, doi:10.1038/nn.4171 (2015).

95 Romero-Garcia, R. *et al.* Structural covariance networks are coupled to expression of genes enriched in supragranular layers of the human cortex. *Neuroimage* **171**, 256-267, doi:10.1016/j.neuroimage.2017.12.060 (2018).

96 Fulcher, B. D., Little, M. A. & Jones, N. S. Highly comparative time-series analysis: the empirical structure of time series and their methods. *J R Soc Interface* **10**, 20130048, doi:10.1098/rsif.2013.0048 (2013).

97 Fagerberg, L. *et al.* Analysis of the human tissue-specific expression by genome-wide integration of transcriptomics and antibody-based proteomics. *Mol Cell Proteomics* **13**, 397-406, doi:10.1074/mcp.M113.035600 (2014).

98 Sun, D. *et al.* Large-scale mapping of cortical alterations in 22q11.2 deletion syndrome: Convergence with idiopathic psychosis and effects of deletion size. *Mol Psychiatry* **25**, 1822-1834, doi:10.1038/s41380-018-0078-5 (2020).

99 Hoogman, M. *et al.* Brain Imaging of the Cortex in ADHD: A Coordinated Analysis of Large-Scale Clinical and Population-Based Samples. *The American journal of psychiatry* **176**, 531-542, doi:10.1176/appi.ajp.2019.18091033 (2019).

100 van Rooij, D. *et al.* Cortical and Subcortical Brain Morphometry Differences Between Patients With Autism Spectrum Disorder and Healthy Individuals Across the Lifespan: Results From the ENIGMA ASD Working Group. *The American journal of psychiatry* **175**, 359-369, doi:10.1176/appi.ajp.2017.17010100 (2018).

101 Whelan, C. D. *et al.* Structural brain abnormalities in the common epilepsies assessed in a worldwide ENIGMA study. *Brain* **141**, 391-408, doi:10.1093/brain/awx341 (2018).

102 Schmaal, L. *et al.* Cortical abnormalities in adults and adolescents with major depression based on brain scans from 20 cohorts worldwide in the ENIGMA Major Depressive Disorder Working Group. *Mol Psychiatry* **22**, 900-909, doi:10.1038/mp.2016.60 (2017).

103 Boedhoe, P. S. W. *et al.* Cortical Abnormalities Associated With Pediatric and Adult Obsessive-Compulsive Disorder: Findings From the ENIGMA Obsessive-Compulsive Disorder Working Group. *The American journal of psychiatry* **175**, 453-462, doi:10.1176/appi.ajp.2017.17050485 (2018).

104 van Erp, T. G. M. *et al.* Cortical Brain Abnormalities in 4474 Individuals With Schizophrenia and 5098 Control Subjects via the Enhancing Neuro Imaging Genetics Through Meta Analysis (ENIGMA) Consortium. *Biol Psychiatry* **84**, 644-654, doi:10.1016/j.biopsych.2018.04.023 (2018).

105 Hibar, D. P. *et al.* Cortical abnormalities in bipolar disorder: an MRI analysis of 6503 individuals from the ENIGMA Bipolar Disorder Working Group. *Mol Psychiatry* **23**, 932-942, doi:10.1038/mp.2017.73 (2018).

106 Opel, N. *et al.* Brain structural abnormalities in obesity: relation to age, genetic risk, and common psychiatric disorders : Evidence through univariate and multivariate mega-analysis including 6420 participants from the ENIGMA MDD working group. *Mol Psychiatry* **26**, 4839-4852, doi:10.1038/s41380-020-0774-9 (2021).

107 Kirschner, M. *et al.* Cortical and subcortical neuroanatomical signatures of schizotypy in 3004 individuals assessed in a worldwide ENIGMA study. *Mol Psychiatry* **27**, 1167-1176, doi:10.1038/s41380-021-01359-9 (2022).

108 Laansma, M. A. *et al.* International Multicenter Analysis of Brain Structure Across Clinical Stages of Parkinson's Disease. *Mov Disord* **36**, 2583-2594, doi:10.1002/mds.28706 (2021).

109 Vasa, F. & Misic, B. Null models in network neuroscience. *Nature reviews. Neuroscience*, doi:10.1038/s41583-022-00601-9 (2022).